Chapter 6

Results and discussions

6.1 Defects in ZnO

Introduction

ZnO occurs naturally as an n-type semiconductor. This n-type conductivity is attributed to native defects and impurities introduced into the material during growth. During material growth, impurities introduce energy states in the forbidden region within the bandgap of the semiconductor. Depending on their location within the ZnO bandgap, these impurities can be classified as either shallow levels or deep level defects. Characterization of these defects can be performed using several techniques. In this thesis, the Hall effect and DLTS techniques were used to characterize defects. This section gives an outline of the defects observed in as-received bulk single crystal ZnO using DLTS.

Results and discussions

The DLTS spectrum obtained from the as-received ZnO samples using conventional DLTS is shown in Figure 6.1.1.

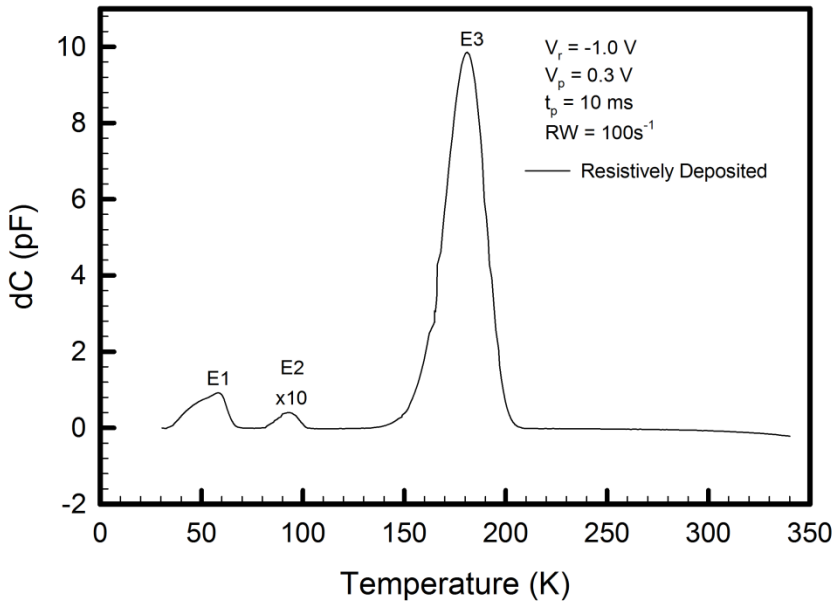

Figure 6.1.1: DLTS spectrum obtained from the as-received melt grown single crystal ZnO obtained from Cermet. The spectrum was obtained at a quiescent reverse bias of 1.0 V, filling pulse width of 10 ms, pulse height, V_p = 0.3 V and rate window of 100 s^{-1}.

To facilitate the use of DLTS, Pd Schottky contacts were resistively deposited on ZnO as it has been observed that this technique does not introduce defects in ZnO [1]. Defects labelled E1 and E3 have been observed in material grown using different techniques. This clearly indicates that these defects are common to ZnO regardless of the growth, processing and contact fabrication techniques [2, 3, 4, 5]. However, the E2 defect has not been reported by many as it has not been observed in some other ZnO materials. Hence this defect might be growth technique related. The Arrhenius plots to determine the estimated activation enthalpies of the E1, E2 and E3 deep level defects are shown in Figure 6.1.2.

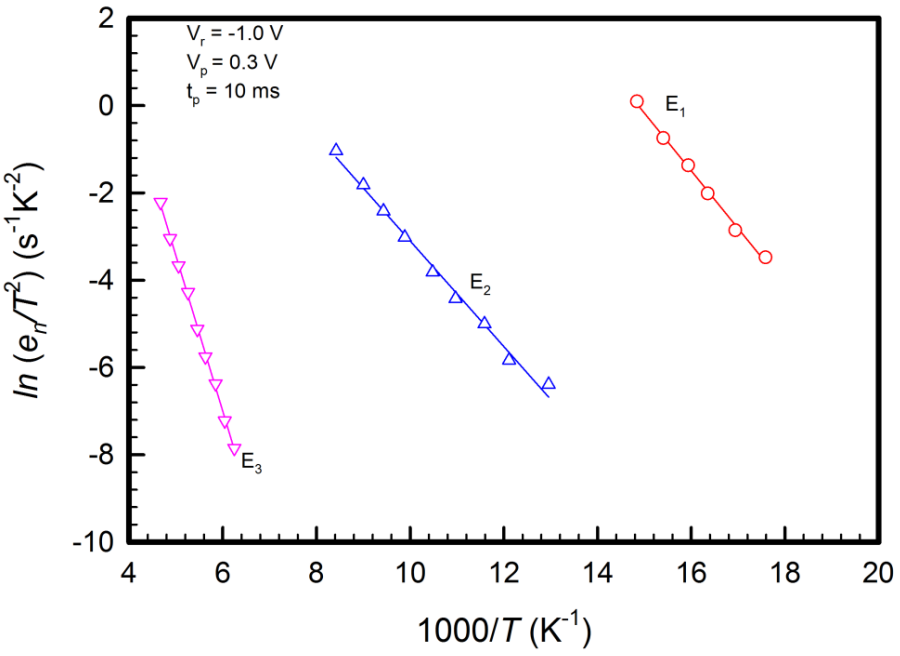

Figure 6.1.2: Arrhenius plots for the as–received melt grown bulk single crystal ZnO.

From the DLTS spectrum of Figure 6.1.1, the E1 peak is asymmetric. This could be due to the fact that it is observed very close to the freeze out region. The *C-T* scan showing the freeze out region of ZnO is shown in Figure 6.1.3.

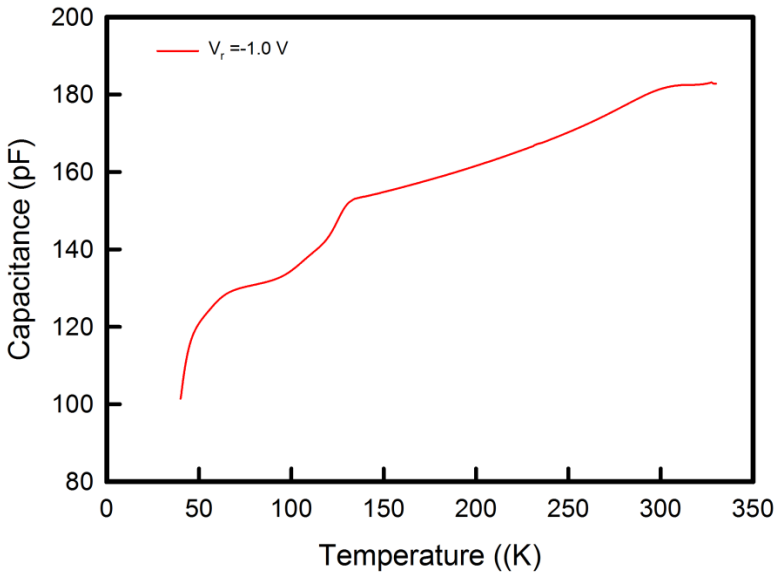

Figure 6.1.3: Capacitance-temperature scan for the as–received melt grown bulk single crystal ZnO. This scan was recorded at a constant reverse bias voltage of 1.0 V, scanning up in temperature.

The freeze out region of ZnO starts occurring at a temperature of about 50 K. The location of the E1 peak near the freeze out region can also influence the accurate determination of its

activation enthalpy. Due to this effect, values ranging from 0.11 – 0.12 eV have been reported for the activation enthalpy of the E1 peak.

Values of estimated activation enthalpies, apparent capture cross-sections and possible identities of these defects are shown in Table 6.1.1. Material growth techniques are also included.

Table 6.1.1. *Values of estimated activation enthalpy, apparent capture cross-section and possible identities of the deep level defects observed in ZnO.*

Defect label	Material Growth technique*	Activation enthalpy (eV)	Apparent capture cross section (cm^2)	Identity	Ref
E1	*PLD	0.10	?	?	[2]
	*MG	0.111	5.2×10^{-12}	O_i?	[3]
	*SCVT	0.12	?	?	[4]
	MG	0.12	?	?	[4]
	Vapour phase	0.12	2.7×10^{-13}	?	[5]
E2	MG	0.110	1.23×10^{-16}	?	[1]
	SCVT	0.10	1×10^{-17}	?	[4]
E3	PLD	0.31	5×10^{-16}	?	[6]
	Hydrothermal	0.30	2.0×10^{-15}	O_2 deficiency	[7]
	Hydrothermal	0.29	2.6×10^{-14}	V_O	[8]
	SCVT	0.29	1.0×10^{-15}	V_O?	[4]
	MG	0.30	2.7×10^{-14}	Transition metal ion related?	[1]
	MG	0.29	1.0×10^{-15}	V_O?	[4]
	Vapour phase	0.29	5.8×10^{-16}	?	[5]
	PLD	0.30	?	?	[2]
	SCVT	0.30	?	?	[9]
	PLD	0.30	2.6×10^{-16}	Transition metal ion related	[10]

*PLD refers to Pulsed Laser Deposition,

*MG refers to Melt growth,

*SCVT refers to Seeded Chemical Vapour Transport

The E1 deep level shows strong electric field dependence which results in electric field enhanced emission effects as shown in Figure 6.1.4. Such an effect has also been reported by [11, 12].

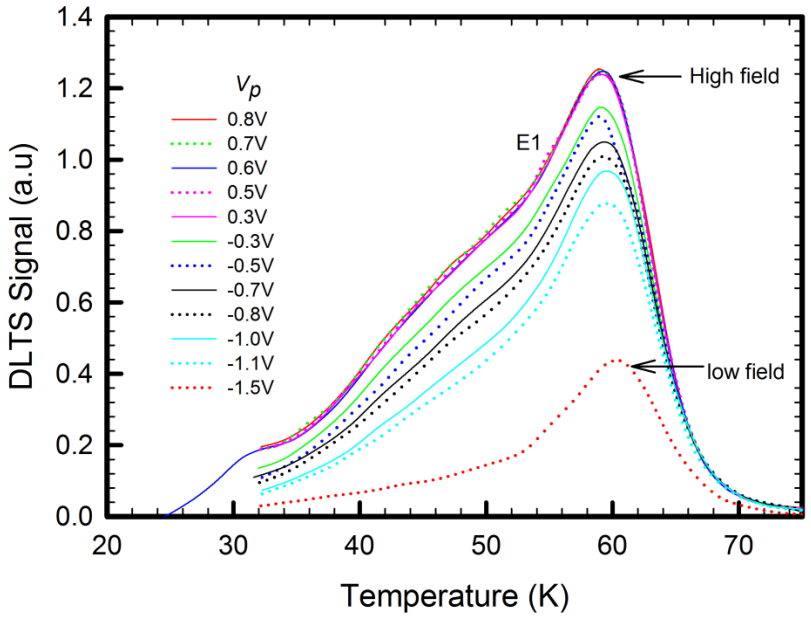

Figure 6.1.4: DLTS spectra showing the electric field dependence of the E1 defect at a rate window frequency of 100Hz, reverse bias voltage of 2.0 V, and filling pulse width of 2.0 ms.

Based on the summary presented in Table 6.1.1, it can be clearly observed that the identities of the native defects in ZnO are not clear yet. However the only valid conclusion is that ZnO contains the E1 and E3 defects independent of the technique used for material growth.

Of particular interest from this study is the behaviour of the E3 defect. The capacitance transients are observed to be non-exponential and also the DLTS peak height shows a significant dependence on rate window frequency. Using shorter filling pulse widths, the peak height increases with increase in rate window. Using large filling pulse widths, the DLTS peak height for all rate window frequencies is the same. This behaviour has been attributed to the temperature dependence of the capture cross-section due to a capture barrier which electrons from a trap level have to overcome to be re-emitted back to the conduction band. A detailed analysis of the behaviour of E3 is given in the attached publication.

Publication 1: On the temperature dependence of the electron capture cross-section of the E3 deep level observed in single crystal ZnO

On the temperature dependence of the electron capture cross-section of the E3 deep level observed in single crystal ZnO

Wilbert Mtangi[1], Matthias Schmidt[1], P. Johan Janse van Rensburg[1], Walter E. Meyer[1], Danie F. Auret[1], Jacqueline M. Nel[1], Mmantsae Diale[1], Albert Chawanda[2]

1 Department of Physics, University of Pretoria, Private bag X20, 0028 Hatfield, South Africa
2 Midlands State University, Private Bag, 9055 Senga Gweru, Zimbabwe

E-mail: wilbert.mtangi@up.ac.za

Abstract. We report on the temperature dependence of the capture cross-section of the E3 deep level defect observed in single crystal ZnO samples. Temperature dependent deep level transient spectroscopy reveals an increase in the DLTS peak height with an increase in the rate window frequency for the E3 level which is a proof that the E3 deep level has a temperature activated capture cross-section. However the observed capture rate is not constant during the filling pulse but depends on the occupancy of the defect itself. This phenomenon is in contradiction with what is expected of an ideal deep level.

1. Introduction

ZnO is a wide and direct bandgap semiconductor with experimental bandgap energy of about 3.4 eV. Deep level transient spectroscopy (DLTS) measurements performed on differently grown ZnO crystals reveal the presence of the E3 deep level defect with an activation enthalpy of between 0.29 eV and 0.31 eV and an apparent capture cross-section of 5×10^{-16} cm^2 to 10^{-14} cm^2 [1, 2, 3, 4, 5, 6]. However its ionisation energy as well as its energy barrier for electron capture is not known yet, whereas in established semiconductors such as GaAs and Si, capture barrier energies for most defect levels are well known. The capture barrier is usually obtained using emission rate DLTS scans and varying the filling pulse width as suggested by Henry and Lang [7]. A second method which uses DLTS rate window scans with short filling pulses (less than 10 μs) has been employed by Zhao *et al.* [8], Criado *et al.* [9], Telia *et al.* [10] and Cavalcoli *et al.* [11]. In this paper, we report on the electronic properties of the E3 deep level in a bulk single crystal ZnO sample obtained from Cermet Inc.

2. Sample preparation

In preparation of the DLTS measurements, crystal cleaning was performed as in reference [12]. Ohmic contacts with a composition of Al/Au were deposited on the O-polar face using the resistive evaporation technique at a pressure of approximately 10^{-6} Torr. Finally, Iridium Schottky contacts with a diameter of 0.5 mm and thickness of 100 nm were electron beam deposited onto the Zn-polar face under vacuum at a pressure of approximately 10^{-7} Torr.

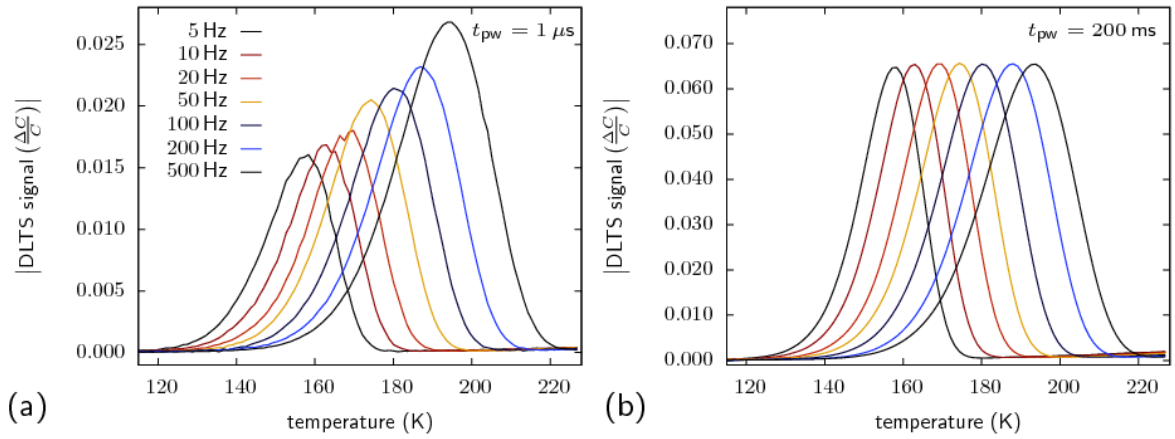

Figure 1. The E3 peak in deep level transient spectroscopy temperature scans conducted at different rate window frequencies using 1 μs filling pulses (a) and 200 ms filling pulses (b) that flattened the bands. During the recording of the capacitance transients the sample was reverse biased at 2 V.

Current voltage measurements at room temperature confirmed that the sample was suitable for DLTS measurements and a net doping density of $N_{\mathsf{net}} = 4.6 \times 10^{16}\,\mathrm{cm}^{-3}$ was obtained from CV measurements using the van Opdorp analysis [13].

3. Results and discussion

Emission DLTS rate window scans were performed in the dark in a closed cycle helium cryostat and revealed the presence of the E3 deep level, as shown in Figure 1. Arrhenius analysis[1] of the temperature dependence of the thermal emission rate of the E3 level yielded an activation enthalpy of 0.30 eV and an apparent capture cross-section of $10^{-14}\,\mathrm{cm}^2$. It was observed that the spectra differ depending on the filling pulse width (t_{pw}). For $t_{\mathsf{pw}} = 1\mu$s filling (Figure 1(a)), the DLTS peak height increases with an increase in rate window frequency, whereas for long enough filling pulse widths (Figure 1(b)), the peak height was constant for all rate window frequencies. The variation of the DLTS peak height with chosen rate window frequency for the E3 deep level has previously been observed but to the best of our knowledge, no explanation was given. In the following we are going to shed some light on this observed effect. The DLTS experiment allows one to prepare an initial probability to find a defect state occupied by an electron, q_{in}. This is achieved by the application of a filling pulse and monitoring the capacitance transient afterwards. The DLTS signal peak height, $\Delta C/C$ is related to the trap concentration N_{t} and the difference in the occupancy probabilities by,

$$\frac{\Delta C}{C} = -\frac{N_{\mathsf{t}}}{2N_{\mathsf{net}}}\left(q_{\mathsf{fin}} - q_{\mathsf{in}}\right) \tag{1}$$

where q_{fin} is the final occupation probability. The differential equation for the time evolution of the occupancy probability $q(t)$ of a defect state is [14]

$$\frac{\mathrm{d}q(t)}{\mathrm{d}t} = c_{\mathsf{n}}\left[1 - q(t)\right] - e_{\mathsf{n}}^{\mathsf{th}} q(t). \tag{2}$$

[1] ZnO effective mass: 0.27 m_{e}

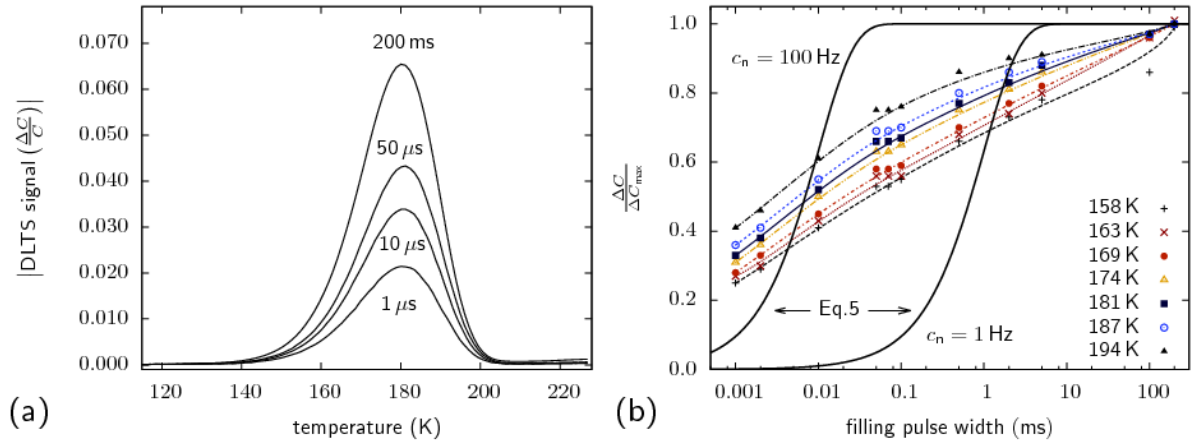

Figure 2. a) Dependence of the E3 DLTS peak height on filling pulse width t_{pw} at a rate window frequency of 100 Hz. b) Symbols represent the variation of the measured, normalised DLTS peak height with filling pulse width and sample temperature. The black solid lines are the graphical representation of equation 5 assuming a constant capture cross-section during the filling process.

c_n denotes the thermal capture rate for electrons and its temperature-dependence is given by

$$c_n(T) = \sigma_n(T)\,\langle v_{th}\rangle\,(T) n(T) = \sigma_n^{\infty} \exp\left(-\frac{E_b}{k_B T}\right) \langle v_{th}\rangle\,(T) n(T) \tag{3}$$

where E_b is the barrier for electron capture, $\langle v_{th}\rangle\,(T)$ is the thermal velocity of electrons and n is the free electron concentration available for capture. Since at a particular temperature, c_n is considered to be a constant and assuming that during the filling process, $e_n^{th} \ll c_n$, the solution of equation 2 is given by

$$q(t) = 1 - \exp\left(-c_n t\right). \tag{4}$$

Thus, equation 1 can be written as,

$$\frac{\Delta C}{C} = \frac{N_t}{2N_{net}} \left(1 - \exp\left[-c_n t_{pw}\right]\right) \tag{5}$$

since for the maximum DLTS peak height, $q_{fin} \approx 0$.

In the light of this, we studied the filling process of E3 by varying the filling pulse width at fixed rate window frequency. The results are presented in Figure 2(a). As expected, the DLTS peak height increases with increasing filling pulse width as well as increasing temperature, Figure 2(b). However this increase is not in accordance with equation 5 and therefore the Henry and Lang approach [7] cannot be applied. In particular, the slope of the measured, normalised DLTS peak height versus filling pulse width plot is less steep compared to the one predicted by equation 5. A suggestion of this is as follows.

Since every solution of equation 2 must be exponential if c_n and e_n^{th} are constant, only a change of c_n during the filling process can explain our observations. According to equation 3, this change can be attributed to either a decrease in σ_n (at the same temperature) or a decrease in n in the vicinity of the defect while it is being filled. The first possibility might originate from defect-defect interaction which cannot be excluded at doping levels of $N_{net} = 4.6 \times 10^{16}\,\mathrm{cm}^{-3}$. The latter, which to our opinion might be more probable, is due to the charging up of grain

boundaries. This results in a double Schottky barrier and therefore a depletion region which lowers the local electron density [15]. Further investigations and analysis are required and will be performed.

4. Conclusions

In conclusion, the electron capture of the E3 deep level in ZnO was studied in detail by DLTS. The capture process cannot be described by a single exponential filling of the defect state, as would be the case for a simple capture barrier of an isolated point defect. Due to this difficulty, the capture barrier could not be obtained from emission DLTS rate window scans with varying pulse widths without employing a more involved analysis. Furthermore there is a high uncertainty associated with the high temperature limit of the capture cross-section obtained from standard Arrhenius analysis which is frequently reported.

Acknowledgments

The authors wish to thank the University of Pretoria for the financial support. Matthias Schmidt was funded by the Postdoctoral Fellowship Program of the University of Pretoria. This work is based upon research supported by the National Research Foundation (NRF). Any opinion, findings and conclusions or recommendations expressed in this material are those of the author(s) and therefore the NRF does not accept any liability in regard thereto.

References

[1] F.D. Auret, S.A. Goodman, M.J. Legodi, W.E. Meyer, and D.C. Look. *Electrical characterization of vapor-phase-grown single-crystal ZnO.* Appl. Phys. Lett., **80** 1340–1342, (2002).

[2] A.Y. Polyakov, N.B. Smirnov, A.V. Govorkov, E.A. Kozhukhova, S.J. Pearton, D.P. Norton, A. Osinsky, and A. Dabrian, *Electrical Properties of Undoped Bulk ZnO Substrates.* J. Electron. Mater., **35** 663-669, (2006)

[3] F.D. Auret, W.E. Meyer, P.J. Janse van Rensburg, M. Hayes, J.M. Nel, H. von Wenckstern, H. Schmidt, G. Biehne,H. Hochmuth, M. Lorenz, M. Grundmann, *Electronic properties of defects in pulsed-laser deposition grown ZnO with levels at 300 and* 370 meV *below the conduction band.* Physica B, **401-402** 378-381 (2007)

[4] H. von Wenckstern, K. Brachwitz, M. Schmidt, C.P. Dietrich, M. Ellguth, M. Stlzel, M. Lorenz and M. Grundmann, *The E3 Defect in MgZnO.* J. Electron. Mater., **39** 584-588, (2010)

[5] W. Mtangi, F.D. Auret, P.J. Janse van Rensburg, S.M.M. Coelho, M.J. Legodi, J.M. Nel, and W.E. Meyer, *A comparative study of the electrical properties of Pd/ZnO Schottky contacts fabricated using electron beam deposition and resistive/thermal evaporation techniques.* J. Appl. Phys., **110** 094504, (2011)

[6] Matthias Schmidt, *Space Charge Spectroscopy Applied to Defect Studies in Zinc Oxide Thin Films*, PhD thesis, Universität Leipzig, Germany (2012).

[7] C.H. Henry and D.V. Lang, *Nonradiative capture and recombination by multiphonon emission in GaAs and GaP.* Phys. Rev. B **15** 989-1016 (1977).

[8] J.H. Zhao, T.E. Schlesinger, and A.G. Milnes, *Determination of carrier capture cross sections of traps by deep level transient spectroscopy of semiconductors.* J. Appl. Phys. **62** 2865–2870 (1987).

[9] J. Criado, A. Gomez, E. Muñoz, and E. Calleja, *Novel method to determine capture crosssection activation energies by deeplevel transient spectroscopy techniques.* Appl. Phys. Lett. **52** 660-661 (1988).

[10] A. Telia, B. Lepley, and C. Michel, *Experimental analysis of temperature dependence of deeplevel capture crosssection properties at the Au oxidized InP interface.* J. Appl. Phys. **69** 7159-7165 (1991).

[11] D. Cavalcoli, A. Cavallini, E. Gombia, *Anomalous temperature dependence of deep-level-transient-spectroscopy peak amplitude.* Phys. Rev. B **56** 14890-14892 (1997).

[12] W. Mtangi, F.D. Auret, C. Nyamhere, P.J. Janse van Rensburg, M. Diale, and A. Chawanda, *Analysis of temperature dependent I-V measurements on Pd/ZnO Schottky barrier diodes and the determination of the Richardson constant.* Physica B **404** 1092-1096 (2009).

[13] C. van Opdorp. *Evaluation of doping proles from capacitance measurements.* Solid State Electron., **11** 397 (1968).

[14] P. Blood and J.W. Orton. *The Electrical Characterization of Semiconductors: Majority Carriers and Electron States*, volume 1. Academic Press, US, 1992.

[15] F. Greuter and G. Blatter, *Electrical properties of grain boundaries in polycrystalline compound semiconductors.* Semicond. Sci. Technol. **5** 111-137 (1990).

Summary

As-grown melt grown single crystal ZnO samples contain three prominent deep level defects, E1, E2 and E3. The E1 and E3 deep levels are observed in material grown using different techniques. This indicates that these defects are common in ZnO. However, the identity of these particular defects is not known yet. The E2 defect has been observed to be dependent on material growth technique as it has not been observed in all the other materials grown using other techniques except in SCVT and melt grown samples used in this study. From the temperature dependence of the capture cross-section of the E3 peak, a capture barrier energy could not be calculated using the approach by Henry and Lang [13]. This is due to the fact that the capture process of the E3 could not be described by a single exponential filling of a defect state as would be the case for a simple capture barrier of an isolated point defect.

References

1. W. Mtangi, F. D. Auret, P. J. Janse van Rensburg, S. M. M. Coelho, M. J. Legodi, J. M. Nel, W. E. Meyer, and A. Chawanda, J. Appl. Phys. **110**, 094504 (2011)
2. M. Grundmann, H.von. Wenckstern, R. Pickenhain, Th. Nobis, A. Rahm, M. Lorenz, Superlattices and Microstruct. **38**, 317 (2005)
3. W. Mtangi, F. D. Auret, W. E. Meyer, M. J. Legodi, P. J. Janse van Rensburg, S. M. M. Coelho, M. Diale, and J. M. Nel, J. Appl. Phys. **111**, 094504 (2012)
4. F. D. Auret, J. M. Nel, M. Hayes, L. Wu, W. Wesch, E. Wendler, Superlattices and Microstruct. **39**, 17 (2006)
5. F. D. Auret, S. A. Goodman, M. Hayes, M. J. Legodi, H. A. van Laarhoven, and D. C. Look, Appl. Phys. Lett. **79**, 3074 (2001)
6. H. von Wenckstern, R. Pickenhain, H. Schmidt, M. Brandt, G. Biehne, M. Lorenz, M. Grundmann, and G. Brauer, Appl. Phys. Lett. **89**, 092122 (2006)
7. V. Quemener, L. Vines, E. V. Monakhov, and B. G. Svensson, Int. J. Appl. Ceram. Technol. **8**, 1017 (2011)
8. J. C. Simpson, and J. F. Cordaro, J. Appl. Phys. **63**, 1781 (1988)
9. A. Y. Polyakov, N. B. Smirnov, E. A. Kozhukhova, V. I. Vdovin, K. Ip, Y. W. Heo, D. P. Norton, and S. J. Pearton, Appl. Phys. Lett. **83**, 1575 (2003)
10. H. von Wenckstern, G. Biehne, M. Lorenz, M. Grundmann, F. D. Auret, W. E. Meyer, P. J. Janse van Rensburg, M. Hayes and J. M. Nel, J. Korean Physical Society, **53**, 2861 (2008)
11. F. D. Auret, S. A. Goodman, M. Hayes, M. J. Legodi, H. A. van Laarhoven, and D. C. Look, J. Phys.:Condens. Matter. **13**, 8989 (2001)
12. W. Mtangi, F. D. Auret, C. Nyamhere, P. J. Janse van Rensburg, M. Diale, and A. Chawanda, Physica B, **404**, 1092 (2009)
13. C. H. Henry and D. V. Lang, Phys. Rev. B, **15**, 989 (1977)

6.2 Electron-beam induced defects

Introduction

Fabrication of stable rectifying contacts on ZnO has been a problem since the early discovery of the material. Of late reports on highly stable and rectifying contacts on ZnO have been published after hydrogen peroxide treatment [1,2,3,4]. Of concern is the quality of the contacts in terms of barrier height, reverse current, degree of rectification and dominant current transport mechanisms. Some reports have indicated the dependence of contact quality on metal work functions where the focus has been on measured barrier heights. Theoretically, metals with high work functions are expected to produce contacts with high barrier heights. However, reports on metal/ZnO contacts have indicated the independence of barrier heights on metal work functions with most reported barrier heights ranging between 0.60 – 0.80 eV [5,6]. This has been explained as an effect caused by an oxygen vacancy that is situated at an energy level of 0.70 eV below the minimum of the conduction band that pins the ZnO Fermi level and the free energy of metal oxide formation [7].

Other reports have indicated the dependence of contact quality on the deposition technique where focus has been shifted to the defects introduced in the material during contact fabrication. Defects introduced during contact fabrication lead to poor rectification of devices, e.g. reduction in free carrier concentration and high leakage currents. Also of importance is the thermal stability of the contacts. It is expected that metals with high melting points and less reactive should form thermally stable contacts on ZnO. With the potential of fabricating devices that can be used in space applications and the ultraviolet region, i.e. in high temperature and high radiant conditions, thermally stable devices are required.

Reports on the use of Pt and Ir to fabricate thermally stable and highly inert devices have been published [7, 8]. Since Pt and Ir have high melting points, the most likely contact fabrication techniques to be used are the e-beam and sputter deposition, just to mention a few. Auret *et al.* [9] have investigated the effect of e-beam deposition on GaN samples using Ru. Their report indicates the introduction of defects that affect the IV characteristics of the devices. Mtangi *et al.* [10] have reported the introduction of defects in ZnO after e-beam deposition of Pd contacts. In this section, a discussion of the defects introduced in ZnO by e-beam deposition is outlined.

Results and discussions

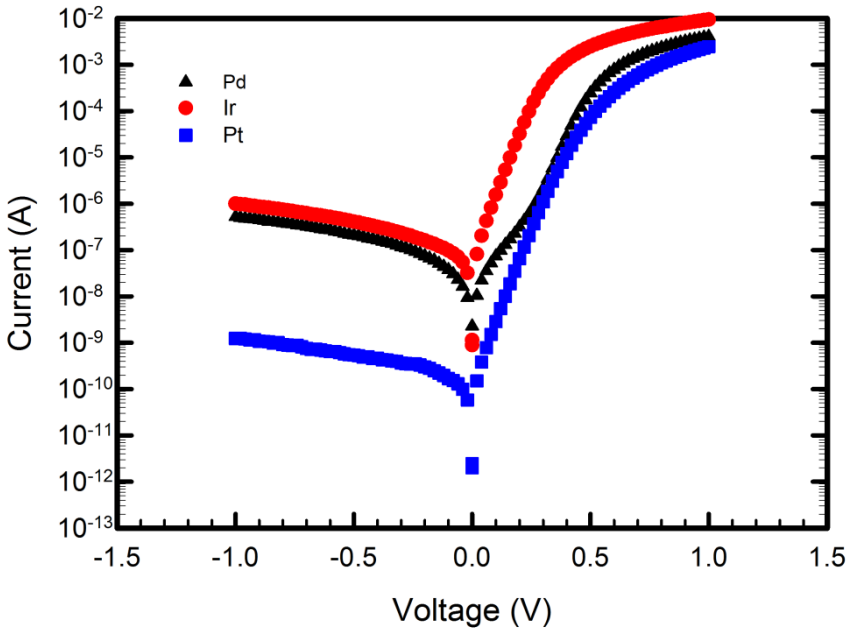

Figure 6.2.1: *A semi-logarithmic IV characteristics of e-beam deposited Schottky contacts measured at 298 K. The dark triangles represent Pd contacts, red circles represent the Ir contacts and the blue squares represent Pt contacts.*

Figure 6.2.1 shows the semi-logarithmic IV plot for the e-beam deposited metal/ZnO contacts obtained at room temperature. Pt contacts reveal a very low reverse current at 1.0 V compared to Pd and Ir contacts. The Pt and Ir contacts reveal the dominance of pure thermionic emission in the voltage range examined while the Pd contacts indicate some generation recombination effects at low voltages, < 0.30 V. The IV characteristics have been analysed by fitting a pure thermionic model to the linear region of the curves. For Pd contacts we have fitted the model to the intermediate region, i.e. 0.30 V < V < 0.50 V. The upper part of the curves shows the dominance of series resistance. Results obtained from fitting a thermionic emission model to the data are shown in Table 6.2.1.

Table 6.2.1: *Values of Schottky barrier height, SBH, ideality factor, series resistance R_s and current at -1.0 V for the e-beam deposited contacts.*

Metal	SBH (eV)	Ideality factor	R_s (Ω)	I (at -1V) (A)
Pd	0.624±0.005	1.66 ± 0.02	110	5.68×10^{-7}
Ir	0.567±0.003	1.28 ± 0.02	70 ± 6	9.09×10^{-7}
Pt	0.710±0.005	1.43 ± 0.04	130 ± 10	1.29×10^{-9}

Pt Schottky contacts indicate a high barrier height compared to Ir and Pd and this justifies the low reverse current measured at 1.0 V while the Ir contacts have a low barrier height, hence the high reverse current measured at 1.0 V. The variation in series resistance can be attributed to the electrical conductivity of the metals. Ir has the highest electrical conductivity of 21.3 x 10^6 S/m, while Pt has the lowest of 9.43 x 10^6 S/m [11], thus the series resistance for the Ir contacts is lower compared to Pd and Pt. Ir contacts also reveal a low ideality factor compared to the Pd and Pt contacts.

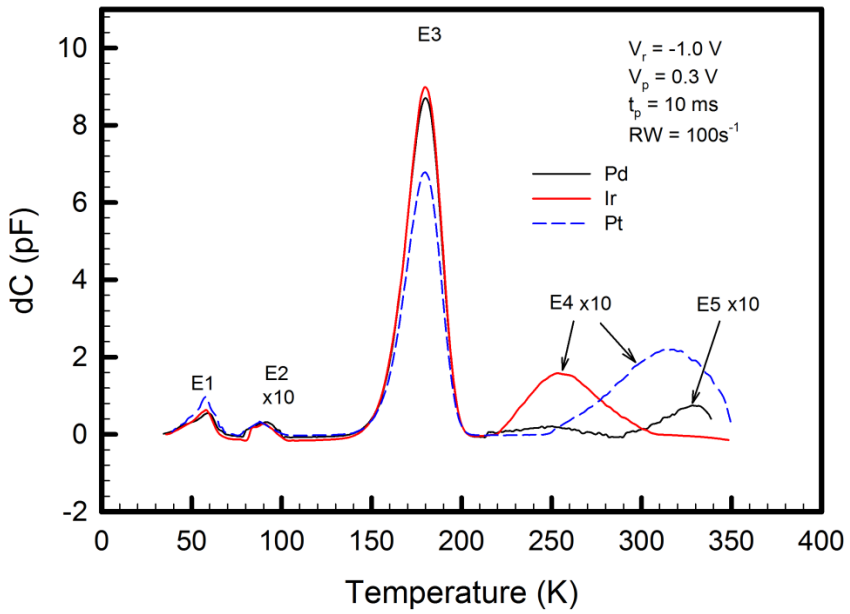

Figure 6.2.2: *DLTS spectra for e-beam deposited samples measured at a quiescent reverse bias of -1.0 V, a filling pulse height, V_p = 0.30 V, filling pulse width of 10 ms and rate window of 100 s^{-1} in the 30 – 350 K temperature range. The dark line represents Pd contacts, red line represents Ir contacts and blue dashed line represents Pt contacts*

Figure 6.2.2 shows the DLTS spectra obtained for the e-beam deposited contacts. All the samples reveal the presence of three prominent peaks as has also been observed and reported by [10,12]. The fourth peak in all samples is the e-beam induced defect [10]. However the peaks are broad indicating that they may consist of two or more energy levels which are closely spaced or defects with a continuous energy distribution as has been observed by Auret *et al*. [13] in GaAs. Figure 6.2.3 shows the Arrhenius plots obtained from the DLTS peaks.

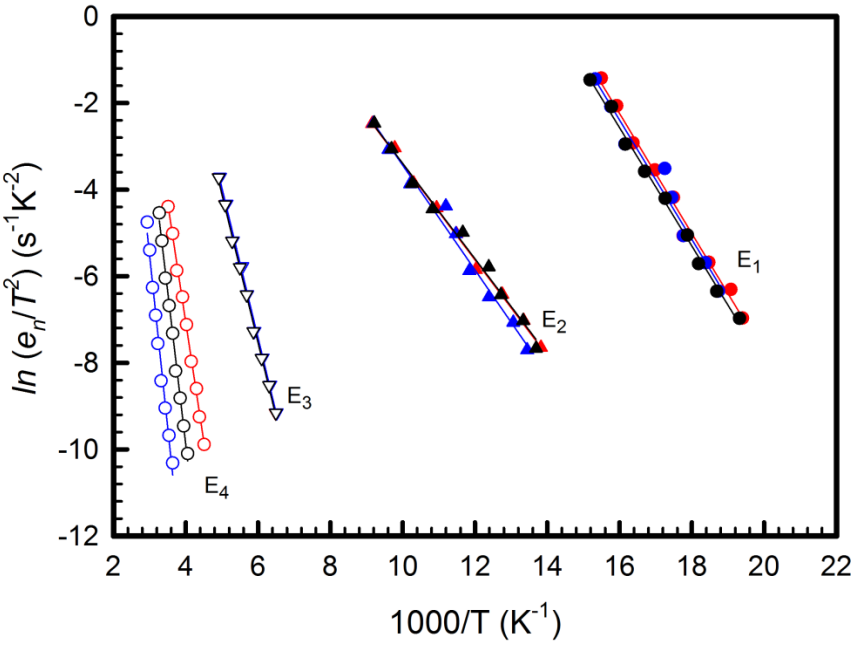

Figure 6.2.3: *Arrhenius plots for the e-beam deposited Schottky contacts. Dark symbols represent Pd contacts, red symbols represent Ir contacts and blue symbols represent Pt contacts.*

The energy levels obtained from the Arrhenius plots together with the estimated capture cross sections are shown in Table. 6.2.2.

Table 6.2.2: *Values of energy levels and capture cross section for the e-beam deposited contacts. Energy levels are measured below the minimum of the conduction band.*

Metal	E1 (eV)	Capture cross section $\times 10^{-12}$ (cm^2)	E2 (eV)	Capture cross section $\times 10^{-17}$ (cm^2)	E3 (eV)	Capture cross section $\times 10^{-15}$ (cm^2)	E4 (eV)	Capture cross section (cm^2)
Pd	0.12	3.73	0.10	3.10	0.30	7.20	0.60	1.43×10^{-12}
Ir	0.12	6.88	0.10	3.27	0.30	8.62	0.48	5.02×10^{-14}
Pt	0.12	5.20	0.10	8.69	0.30	9.48	0.69	1.37×10^{-12}

Defects labelled E1, E2 and E3 can be said to be native to ZnO as they have been observed in ZnO grown by different techniques as has been discussed in the previous section.

The E4 defect that has been introduced during e-beam deposition can be attributed to stray electrons that originate at the filament and are not focused onto the metal since the filament is not a true point source of electrons [9] and also some other negatively charged ionized gas particles. The average energy level for the E4 defect differs significantly from metal to metal. The observed differences might be due to the differences in the chemical nature and energy of the ionized particles that are causing the damage or possibly E4 consists of defects with a

continuous energy distribution. Since the metals used have different melting points, the current used to produce the electron beam so as to melt the metals also varies and thus the particles ionized together with their speeds towards the sample during the deposition process can also vary.

The extent of the damage caused by the ionized particles, has been further investigated by performing a depth profile of the E4 peak. Figure 6.2.4 shows the results obtained from the three samples.

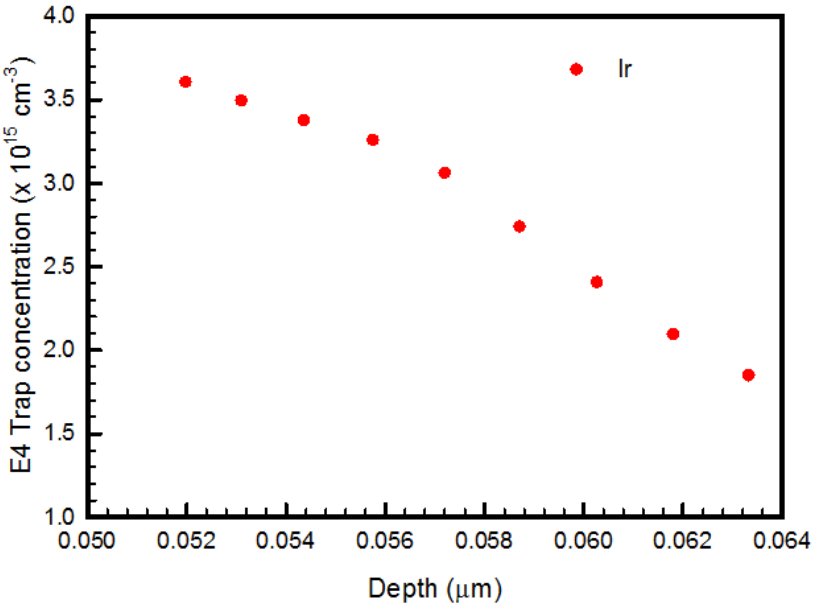

Figure 6.2.4a: *E4 trap concentration versus depth for the Ir Schottky contacts measured at a constant reverse bias of 1.0 V with increasing filling pulse height in steps of 0.05 V*

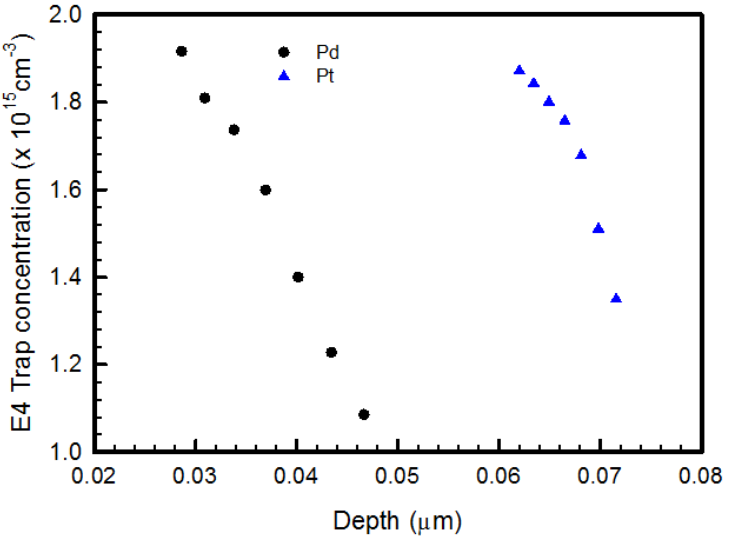

Figure 6.2.4b: *E4 trap concentration versus depth for the Pt and Pd Schottky contacts measured at a constant reverse bias of 1.0 V with increasing filling pulse height in steps of 0.05 V*

The concentration of the E4 defect decreases as we go deeper into the bulk of the semiconductor for all the three metals used. The particles that cause damage during Pd deposition can penetrate a depth shallower than those during Pt and Ir deposition. Since high melting point metals require high current beams compared to those with low melting points, we have higher chances of ionizing more impurities from the metal itself and also those present in the system closer to the filament during deposition. Another possibility is, some ionized metal atoms can gain enough energy during collisions with other particles to cause damage to the ZnO surface [9]. Thus the concentration of the E4 for Ir is higher compared to Pd and Pt. This depth profile was performed at a constant reverse bias of 1.0 V and increasing the pulse height in steps of 0.05 V.

A region of up to 64 nm below the interface has been probed for Ir contacts. The concentration has been observed to decrease from 3.6×10^{15} cm^{-3} at a depth of 52 nm to 1.8×10^{15} cm^{-3} at 64 nm. Using the same measurement conditions, we have managed to probe a region up to 72 nm below the interface for Pt contacts. The concentration has been observed to decrease from 1.9×10^{15} cm^{-3} at 62 nm to 1.3×10^{15} cm^{-3} at 72 nm. For Pd, a depth of 46 nm below the interface has successfully been examined. The concentration has decreased from 1.9×10^{15} cm^{-3} at 29 nm to 1.1×10^{15} cm^{-3} at 46 nm. A similar trend of a decrease in defect concentration with increase in depth has also been observed by [9].

A detailed summary of the e-beam induced defects in ZnO is presented in the article obtained from the link below.

Publication 2: A comparative study of the electrical properties of Pd/ZnO Schottky contacts fabricated using electron beam deposition and resistive evaporation techniques

http://dx.doi.org/10.1063/1.3658027

Summary

Stable rectifying Schottky contacts have been successfully fabricated on ZnO using the electron-beam deposition technique. However, this contact fabrication technique introduces defects on the surface of the material that affect device operation as they contribute to high reverse currents. These deep level defects have successfully been characterized using DLTS. From the defect depth profiling, it has been observed that e-beam deposition introduces defects with high concentrations closer to the surface of the semiconductor. The cause of the E4 defect has been explained as possibly due to ionized impurities from the metals, stray electrons from the filament itself that are not focused towards the metal. These electrons can collide with ionized impurities transferring their energy resulting in impurities impinging onto the sample and also other materials within the system closer to the filament.

References

1. R. Schifano, E. V. Monakhov, B. G. Svensson, S. Diplas, Appl. Phys. Lett. **94**, 132101 (2009)
2. S. Lee, Y. Lee, D. Y. Kim, T W Kang, Appl. Phys. Lett. **96**, 142102 (2010)
3. S.H. Kim, H.K. Kim, S-W Jeong, T-Y Seong, Superlatt. and Microstruct. **39**, 211 (2006)
4. W. Mtangi, F.D. Auret, C. Nyamhere, P.J. Janse van Rensburg, M. Diale, A. Chawanda, Phys. B, **404**, 1092 (2009)
5. U. Ozgur, Y. I. Alivov, C. Lui, A. Teke, M. A. Reshchikov, S. Dogan, V. Avrutin, S. J. Cho, and H. Morkoc, J. Appl. Phys. **98**, 041301 (2005)
6. K. Ip, G. T. Thaler, H. S. Yang, S. Y. Han, Y. J. Li, D. P. Norton, S. J. Pearton, S. W. Jang, and F. Ren, J. Cryst. Growth, **287**, 149 (2006)
7. M. W. Allen, S. M. Durbin, Appl. Phys. Lett. **92**, 122110 (2008)
8. S J Young, L-W Ji, S J Chang, Y P Chen, S-M Peng, Semicond. Sci. Technol. **23**, 085016 (2008)
9. F.D. Auret, S.A. Goodman, G. Myburg, F.K. Koschnick, J.-M. Spaeth, B. Beaumont, P. Gibart, Phys. B, **84**, 273 (1999)
10. W. Mtangi, F.D. Auret, P.J. Janse van Rensburg, S. M. M. Coelho, M. J. Legodi, J.M. Nel, W.E. Meyer, J. Appl. Phys. **110**, 094504 (2011)
11. CRC Handbook of Chemistry and Physics, 80th Edn. 1999-2000
12. F.D. Auret, J.M. Nel, M. Hayes, L. Wu, W. Wesch, E. Wendler, Superlatt. and Microstruct. **39**, 17 (2006)
13. F. D. Auret, G. Myburg, L. J. Bredell, W. O. Barnard, and H. W. Kunert, Mat. Sci. Forum, **83**, 1499 (1992)

6.3 Annealing studies of ZnO using Hall Effect, IV and DLTS

Introduction

Annealing of semiconductor crystals is an important aspect to consider during material processing for device fabrication and characterization. This is due to the fact that it can help recover, activate dopant impurities and in some cases remove defects in crystals that are native or that would have been intentionally introduced. Due to the above-mentioned effects, annealing of crystals results in the modification of the electrical and optical properties of the material and hence fabricated devices. In the case of defects that are already within the material, a study of the annealing kinetics of specific defects can give valuable information on how to improve the efficiency of devices if the optimal conditions have been identified. In ZnO, an effort to identify the nature and origins of the intrinsic defects has been made. Of all the experimental techniques used, none have managed to give the identity of these defects as they have failed to alter the properties of these intrinsic defects. These processes include among others, ion implantation and particle irradiation. Instead, these techniques tend to introduce other electrically active states within the bandgap of the semiconductor. An understanding of the nature of these defects and the origins of the n-type conductivity of the material is essential. This will help in the realization of p-type ZnO since one will have control over the native defects and hence the conductivity of ZnO. Currently, the realization of p-type material is still a challenge since native defects are believed to have self-compensation behaviours. Since the techniques that have been employed have failed to give information to identify the nature of defects in ZnO, one would need to assume that annealing of crystals might give an insight into their identification. However, not much is known about the annealing behaviour of ZnO. In this section, annealing of bulk, melt grown single crystal ZnO samples is studied using the Hall effect, current-voltage and DLTS measurements.

6.3.1 Hall effect studies

Introduction

This technique was employed to characterize the shallow level defects introduced in the material through annealing. This is because the Hall effect technique is a surface sensitive technique. Detailed information pertaining to the study of shallow level defects in ZnO with annealing is obtained from the publication in the link below.

Publication 3: Annealing and surface conduction on hydrogen peroxide treated bulk melt-grown, single crystal ZnO

http://dx.doi.org/10.1016/j.physb.2011.09.101

This publication outlines the experimental procedure used and the results that were obtained together with the conclusions that were drawn from the study.

6.3.2 IV measurements

Introduction

It has been mentioned that annealing affects the electrical properties of devices, such an effect is demonstrated in this section. The results and conclusions drawn from the study are given in the publication obtained from the link below.

Publication 4: Thermal annealing behaviour of Pd Schottky contacts on melt-grown single crystal ZnO studied by IV and CV measurements

http://dx.doi.org/10.1016/j.mseb.2011.10.003

Summary

Annealing of metal/ZnO structures has proved to have an adverse effect on the electrical characteristics of devices. The devices have shown an increase in reverse leakage current with increase in annealing temperature. Annealing the devices at temperatures beyond 550°C results in them losing all their rectification behaviours. An increase in the net doping concentration with increase in annealing temperature has also been observed. The current transport mechanism across the metal/semiconductor interface has been modified from pure thermionic emission to thermionic field emission.

6.3.3 DLTS Studies

Introduction

It has been observed that the Schottky contacts on ZnO lose their rectification behaviour after annealing at high temperatures. At the same time, it has also been mentioned that the depletion layer of the metal/semiconductor interface is modified by annealing. This is a limitation for the determination and characterization of defects in ZnO at high temperatures. In this section, a study on the annealing induced deep level defects in ZnO is performed by annealing the as-received material before contact fabrication. This method allows for the determination of deep level defects even at high annealing temperatures. The Schottky contacts were fabricated after the annealing of the material. This section gives information of deep level defects introduced after annealing the samples in different ambient conditions and temperatures. The results of this study will give an idea of what these defects might relate to by considering those that anneal in or out under the different ambient conditions.

Results and discussions

6.3.3.1 Vacuum annealing

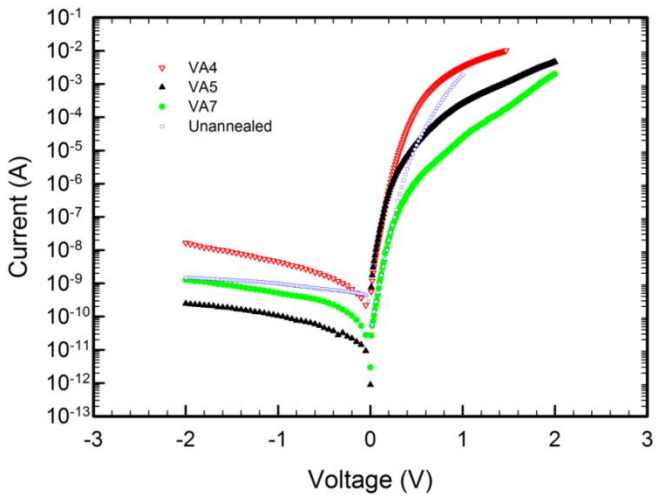

Figure 6.3.3.1.1: Semi-logarithmic IV characteristic of Pd Schottky contacts deposited on vacuum annealed ZnO. The characteristics were recorded at 298 K in the dark.VA4, VA5 and VA7 indicate the annealing temperature of 400°C, 500°C and 700°C, respectively.

Figure 6.3.3.1.1 shows the semi-logarithmic IV characteristics of Pd Schottky contacts deposited on vacuum annealed ZnO samples. It can be clearly observed that annealing modifies the electrical characteristics of the contacts. Parameters extracted from these IV characteristics by fitting the linear region of the forward IV curves are presented in Table 6.3.3.1.1.

Table 6.3.3.1.1: *Average values of Schottky barrier height, SBH, ideality factor, series resistance R_s, and the free carrier concentration from CV depth profile, for the un-annealed and vacuum annealed ZnO samples.*

Annealing Temperature(°C)	SBH (eV) IV	Ideality factor	R_s (Ω)	SBH (eV) CV	N_{dCV} $10^{17}cm^{-3}$
-------	0.721±0.002	1.43 ± 0.01	190	1.16±0.02	2.63±0.03
400	0.58±0.02	1.9 ± 0.3	112±20	1.13±0.02	1.82±0.05
500	0.74±0.05	1.6 ± 0.1	137±30	1.04±0.02	1.48±0.03
700	0.70±0.05	1.3± 0.1	137±20	1.13±0.02	1.94±0.02

Samples annealed at 400°C show a decrease in the average IV barrier height compared to the un-annealed samples. However the barrier height increases after annealing samples at 700°C. For all the annealing temperatures, the average series resistance decreases as compared to the un-annealed sample. This might be due to surface conduction effects in which carriers find an easier path for current flow resulting in low resistance being measured on the samples. The average CV barrier height has been observed to be larger than the IV barrier height. This trend has been observed in many metal/semiconductor contacts and has been explained as due to the influence of thermionic field emission on the charge transport through the interface [1], the existence of an interfacial layer or interface states [2, 3] and also edge leakage currents[4]. From the CV depth profiles, it has been observed that the net doping concentration for all annealing temperatures is less than that of the un-annealed samples.

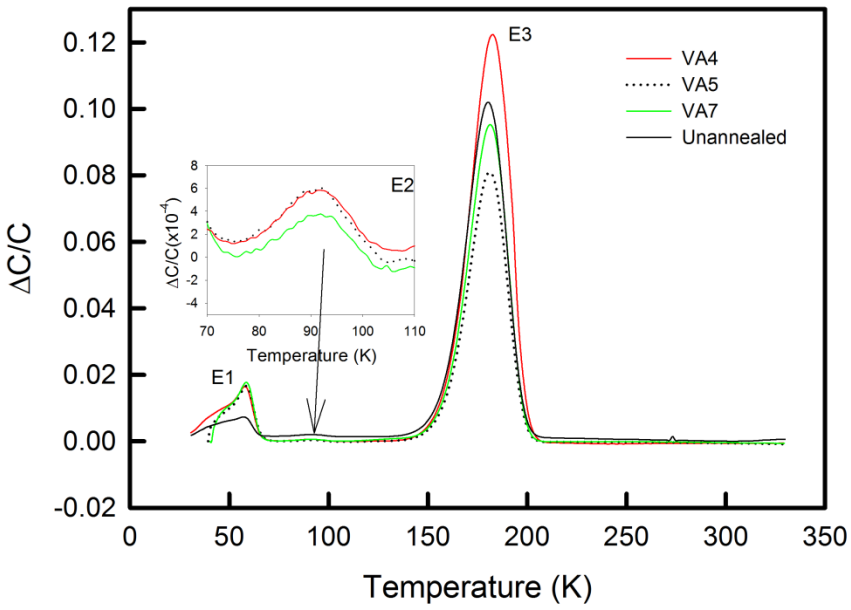

Figure 6.3.3.1.2: DLTS spectra obtained from Pd Schottky contacts deposited on vacuum annealed ZnO. The spectra were recorded at a quiescent reverse bias of -2.0 V, filling pulse of 0.30 V, filling pulse width of 2 ms and rate window of 100s^{-1} in the temperature range 30 – 350 K. VA4, VA5 and VA7 indicate the annealing temperature of 400°C, 500°C and 700°C, respectively. The insert shows the E2 peak.

Figure 6.3.3.1.2 shows the DLTS spectra obtained from the vacuum annealed samples. These spectra were recorded at a rate window of 100 s^{-1}. The annealed samples show three peaks which have been observed in the un-annealed samples. This shows that vacuum annealing does not introduce new defects in bulk-melt grown single crystal ZnO. At the same time, it must be stated that vacuum annealing does not remove deep level defects within the investigated temperature range.

Arrhenius plots shown in Figure 6.3.3.1.3 have been used to extract the defect signatures, i.e. the estimated activation enthalpy and apparent capture cross-section. These values are presented in Table 6.3.3.1.2. The activation enthalpy of the E1 peak has been estimated to be between 94 – 120 meV. This large variation in the activation enthalpy is due to the difficulty in an accurate determination of the value as this defect has a very strong electric field dependence and is also observed very close to the freeze-out region of ZnO indicated in the capacitance temperature scan of Figure 6.3.3.1.4. This defect has been suggested to be Zn vacancy or O_i related [5]. The same explanation can be given for the values of the apparent capture cross-section. The E2 peak has an activation enthalpy that varies from 99 – 103 meV and an apparent capture cross-section of (0.5 – 1) $\times 10^{-16}$ cm^2. Its identity is not known yet.

The E3 peak has an activation enthalpy of 291 – 304 meV and a capture cross-section that varies from (0.5 – 3) $\times 10^{-14}$ cm^2. Its identity is still not clear as illustrated in Table 6.1.1. The E3 peak shows a capture cross-section that is temperature dependent as observed from an increase in the DLTS peak height with increase in rate window frequency.

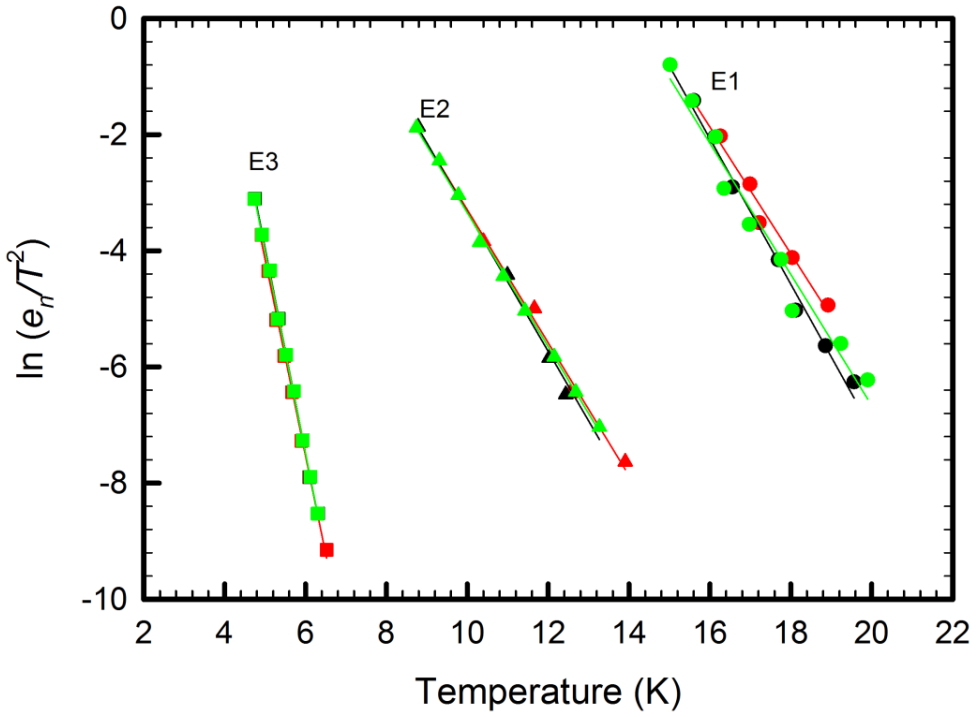

Figure 6.3.3.1.3: Arrhenius plots obtained from Pd Schottky contacts deposited on vacuum annealed ZnO. Red symbols represent samples annealed at 400°C, black symbols are for 500°C annealed samples and green symbols are for the 700°C annealed samples.

Table 6.3.3.1.2: *Values of activation enthalpy and capture cross section for the Pd Schottky contacts deposited on un-annealed and vacuum annealed ZnO. The activation enthalpy is measured relative to the minimum of the conduction band.*

Annealing temperature (°C)	E1 (meV)	Capture cross section (cm^2)	E2 (meV)	Capture cross section (cm^2)	E3 (meV)	Capture cross section (cm^2)
No anneal	120 ± 20	5×10^{-12}	100 ± 20	1×10^{-16}	300 ± 20	3×10^{-14}
400	94 ± 10	9×10^{-14}	99 ± 10	5×10^{-17}	291 ± 10	5×10^{-15}
500	108 ± 10	9×10^{-13}	103± 20	9×10^{-17}	304 ± 20	1×10^{-14}
700	97 ± 10	1×10^{-13}	99 ± 10	5×10^{-17}	301 ± 10	1×10^{-14}

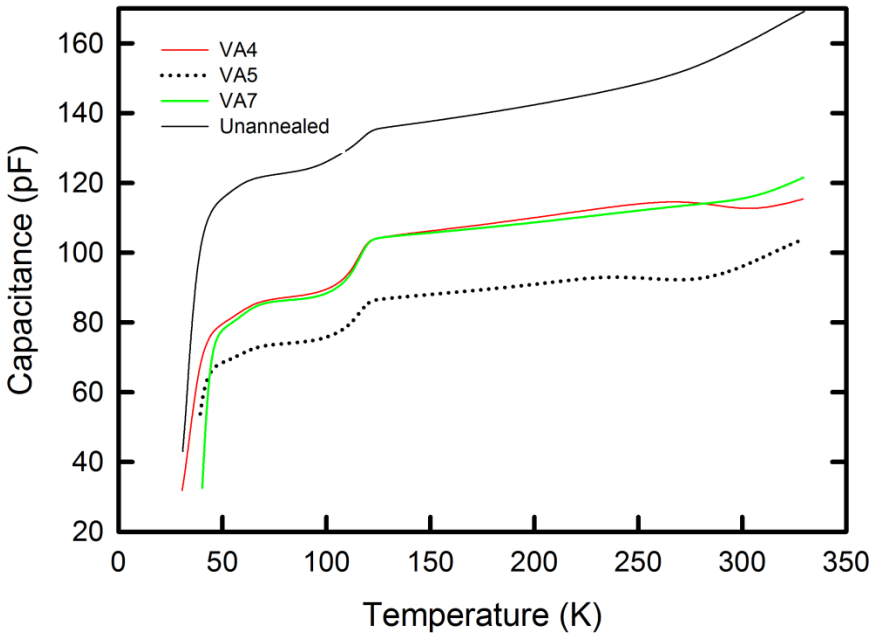

Figure 6.3.3.1.4: Capacitance-temperature scan obtained from Pd Schottky contacts deposited on vacuum annealed ZnO. The spectra were recorded at a quiescent reverse bias of -2.0 V in the temperature range 30 – 350 K. VA4, VA5 and VA7 indicate the annealing temperature of 400°C, 500°C and 700°C, respectively.

Figure 6.3.3.1.4 shows the variation of capacitance with temperature for the vacuum annealed ZnO samples. From these scans, it can be concluded that the freeze-out for ZnO begins around 50 K, where the capacitance drops sharply with a decrease in temperature.

6.3.3.2 Oxygen annealing

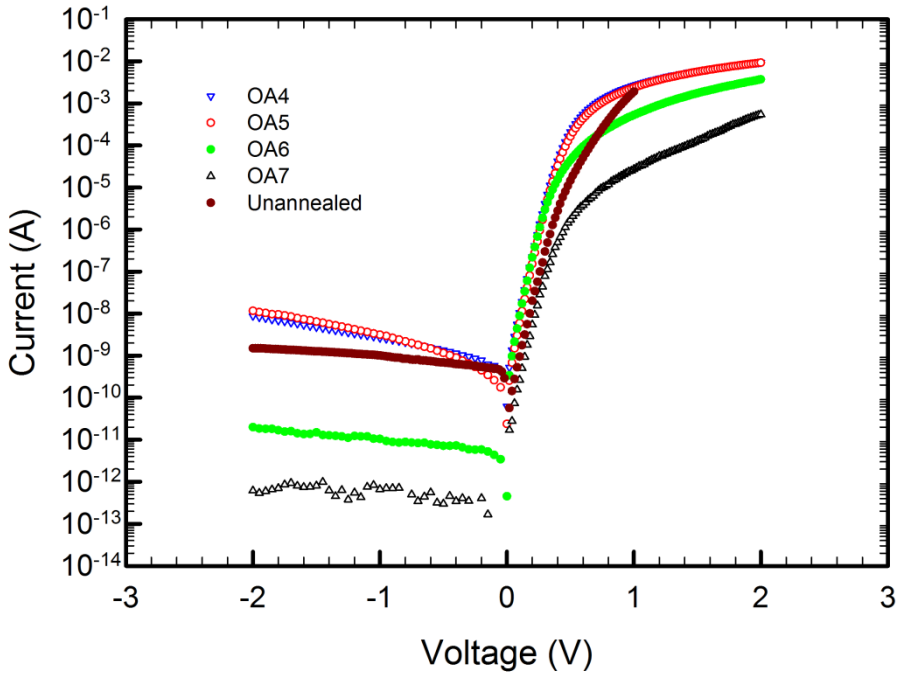

Figure 6.3.3.2.1: Semi-logarithmic IV characteristic of Pd Schottky contacts deposited on oxygen annealed ZnO. The characteristics were recorded at 298 K in the dark.OA4, OA5, OA6 and OA7 indicate the annealing temperature of 400°C, 500°C, 600°C and 700°C, respectively.

The semi-logarithmic IV characteristics for the oxygen annealed ZnO samples indicate a strong dependence on annealing temperature. For the 400°C and 500°C, the characteristics are almost the same to within experimental error. The 700°C annealed samples indicate the lowest leakage current. The leakage current seems to improve with increase in annealing temperature. However, these contacts show a very high series resistance that increases with an increase in annealing temperature. This could be a result of an insulative layer caused by oxygen adsorption during sample annealing. Table 6.3.3.2.1 shows the contact parameters that were obtained from the IV and CV characteristics of the oxygen annealed ZnO samples. As has also been observed with vacuum annealing, the CV barrier height is larger than the average IV barrier height for all annealing temperatures. The net doping concentrations for the annealed samples are also lower compared to that of the as-received samples.

Table 6.3.3.2.1: *Average values of Schottky barrier height, SBH, ideality factor, series resistance R_s, and the free carrier concentration from CV depth profile, for the un-annealed and oxygen annealed ZnO samples.*

Annealing Temperature(°C)	SBH (eV) IV	Ideality factor	R_s (Ω)	SBH (eV) CV	N_{dCV} $10^{17}cm^{-3}$
-------	0.721±0.002	1.43 ± 0.01	190	1.16±0.02	2.63±0.03
400	0.68±0.01	1.44 ± 0.07	143±3	1.09±0.06	1.13±0.04
500	0.65±0.02	1.7 ± 0.2	151±5	0.98±0.04	1.25±0.01
600	0.73±0.02	1.47± 0.06	222±20	1.02±0.03	1.64±0.03
700	0.84±0.02	1.46± 0.06	466±80	1.02±0.02	1.74±0.03

Figure 6.3.3.2.2 shows the DLTS spectra obtained from the oxygen annealed samples. Samples annealed at 400°C, 500°C, 600°C and 700°C indicate the presence of three prominent peaks, similar to those observed in the as-received sample. From the insert shown in the DLTS spectra of Figure 6.3.3.2.3, the 400°C annealed sample shows an extra peak, E4.

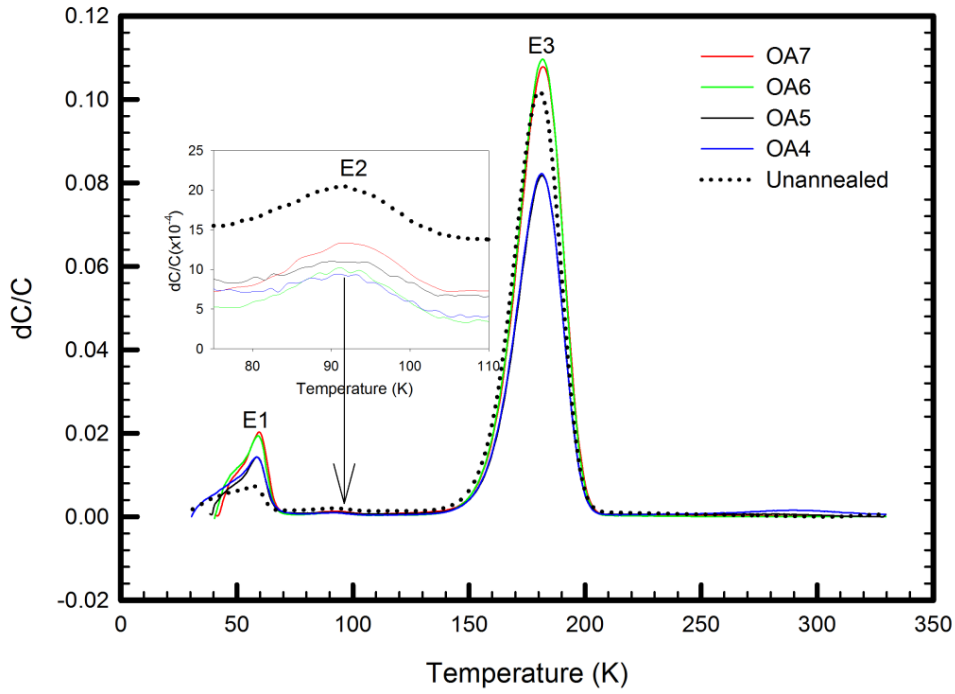

Figure 6.3.3.2.2: DLTS spectra obtained from Pd Schottky contacts deposited on oxygen annealed ZnO. The spectra were recorded at a quiescent reverse bias of -2.0 V, filling pulse of 0.30 V, filling pulse width of 2 ms and rate window of 100s^{-1} in the temperature range 30 – 350 K. OA4, OA5, OA6 and OA7 indicate the annealing temperature of 400°C, 500°C, 600°C and 700°C, respectively. The insert shows the E2 peak.

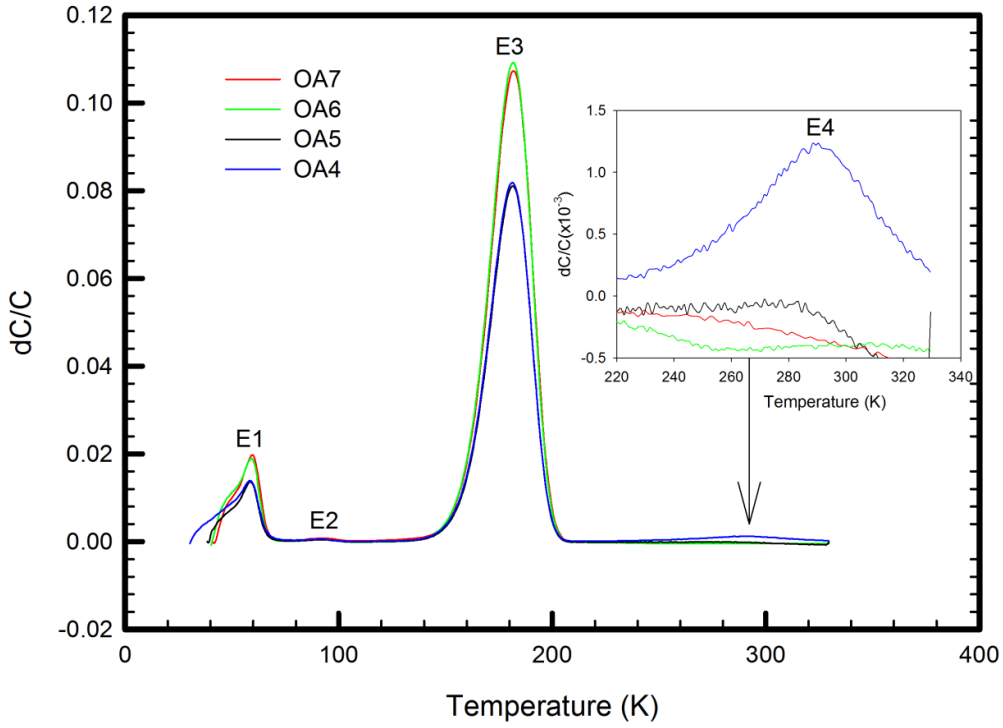

Figure 6.3.3.2.3: DLTS spectra obtained from Pd Schottky contacts deposited on oxygen annealed ZnO. The spectra were recorded at a quiescent reverse bias of -2.0 V, filling pulse of 0.30 V, filling pulse width of 2 ms and rate window of 100 s^{-1} in the temperature range 30 – 350 K. OA4, OA5, OA6 and OA7 indicate the annealing temperature of 400°C, 500°C, 600°C and 700°C, respectively. The insert shows the E4 peak.

The Arrhenius plots shown in Figure 6.3.3.2.4 have been used to calculate the activation enthalpy and apparent capture cross-section for the defects observed in the oxygen annealed ZnO samples. The values obtained from these Arrhenius plots are given in Table 6.3.3.2.2. The activation enthalpy of the E1 defect has been estimated to be 115 – 120 meV and an apparent capture cross-section that varies from $(2 – 5) \times 10^{-12}$ cm^2. E2 with an estimated activation enthalpy of 94 – 100 meV has an apparent capture cross-section of $(0.3 – 1) \times 10^{-16}$ cm^2. As also observed in the vacuum annealed samples, the activation enthalpy of E3 has been estimated to be 294 – 300 meV and an apparent capture cross-section that varies from $(0.7 – 3) \times 10^{-14}$ cm^2. The E4 defect observed in the 400°C annealed samples has an activation enthalpy of 596 meV and an apparent capture cross-section of 4×10^{-14} cm^2. Its identity is not known yet.

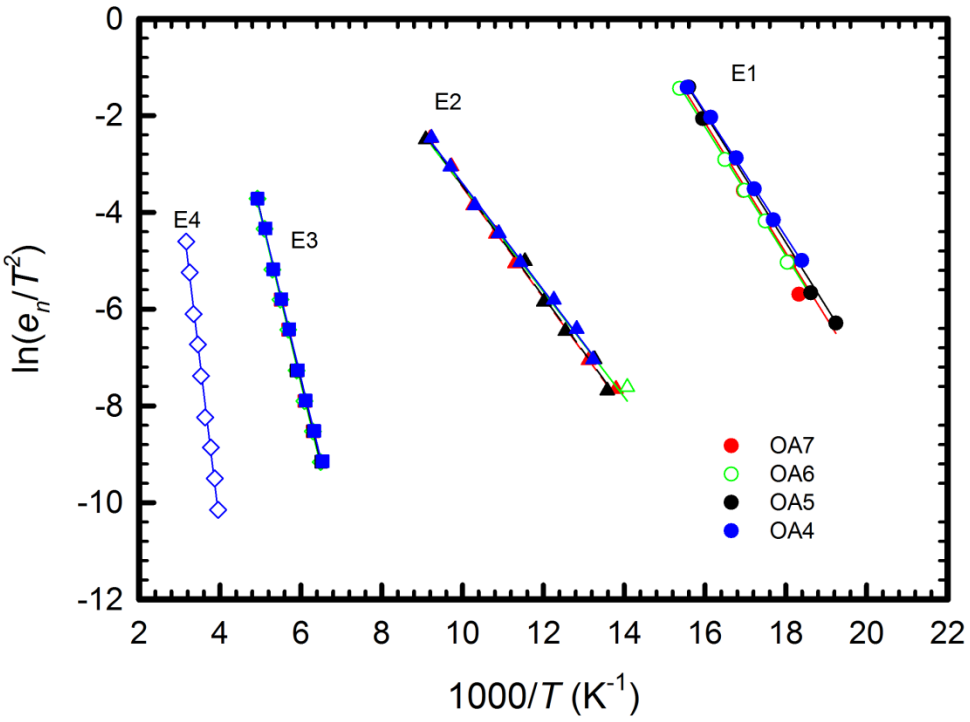

Figure 6.3.3.2.4: Arrhenius plots obtained from Pd Schottky contacts deposited on oxygen annealed ZnO. Red symbols represent samples annealed at 700°C, green symbols are for the 600°C annealed samples, black symbols are for 500°C annealed samples and blue symbols are for the 400°C annealed samples. OA4, OA5, OA6 and OA7 indicate the annealing temperature of 400°C, 500°C, 600°C and 700°C, respectively

Table 6.3.3.2.2: *Values of activation enthalpy and capture cross section for the Pd Schottky contacts deposited on un-annealed and oxygen annealed ZnO. The activation enthalpy is measured relative to the minimum of the conduction band.*

Annealing temperature (°C)	E1 (meV)	Capture cross section (cm^2)	E2 (meV)	Capture cross section (cm^2)	E3 (meV)	Capture cross section (cm^2)	E4 (meV)	Capture cross section (cm^2)
No anneal	120 ± 20	5×10^{-12}	100 ± 10	1×10^{-16}	300 ± 20	3×10^{-14}	-------	---------
400	111 ± 10	2×10^{-12}	95 ± 10	3×10^{-17}	294 ± 20	7×10^{-15}	596 ± 10	4×10^{-13}
500	115 ± 20	4×10^{-12}	99 ± 10	4×10^{-17}	300 ± 20	1×10^{-14}	-------	----------
600	115 ± 20	3×10^{-12}	94 ± 10	3×10^{-17}	300 ± 20	1×10^{-14}	-------	---------
700	116 ± 20	4×10^{-12}	99 ± 10	4×10^{-17}	300 ± 20	1×10^{-14}	-------	---------

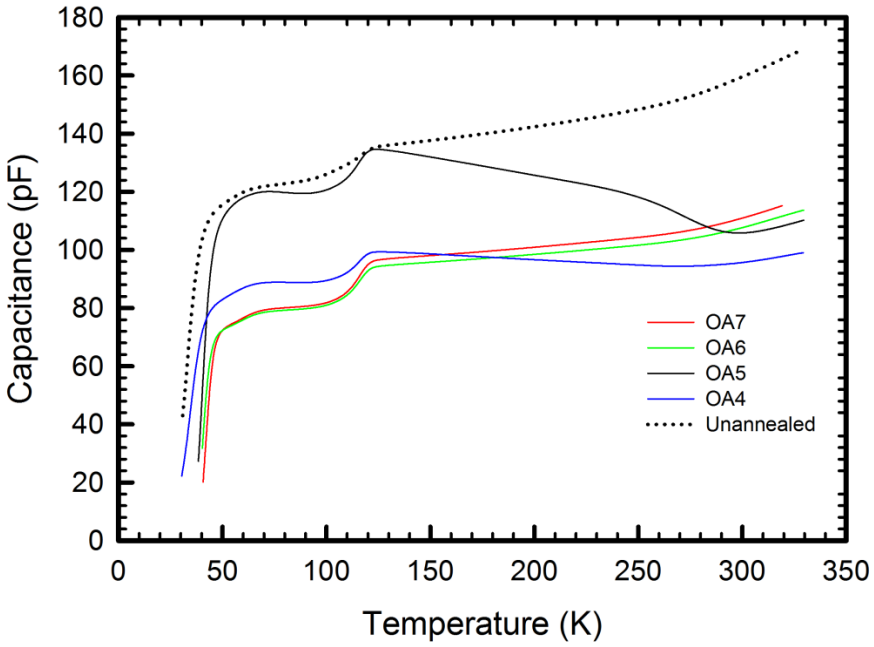

Figure 6.3.3.2.5: Capacitance-temperature scan obtained from Pd Schottky contacts deposited on oxygen annealed ZnO. The spectra were recorded at a quiescent reverse bias of -2.0 V in the temperature range 30 – 350 K. OA4, OA5, OA6 and OA7 indicate the annealing temperature of 400°C, 500°C, 600°C and 700°C, respectively

Figure 6.3.3.2.5 shows the variation of capacitance with temperature for the oxygen annealed ZnO samples. From these scans, it can be concluded that the freeze-out for ZnO begins around 50 K, where the capacitance drops sharply with a decrease in temperature. The Zn_i cannot be observed since the Fermi level is lowered. This lowering is due to the fact that the acceptor concentration for all the annealed samples is now too high, as compared to the concentration of the Zn_i. This is confirmed by the sharp decrease in capacitance in the CT scans. Furthermore, an effective mass donor is formed whose concentration depends on the annealing ambient and temperature, being higher for high annealing temperatures and lower for low annealing temperatures. There is also a possibility that the Zn_i is annealed out and a new shallow donor with high concentration is observed as has been reported by von Wenckstern *et al.* [5] and Mtangi *et al.*[6]. The 400°C and 500°C annealed samples however show a decrease in capacitance with increasing temperature. This has been observed and explained as due to the presence of surface related defects which coexist with deep level defects whose response can only be observed with low frequencies [7].

6.3.3.3 Argon annealing

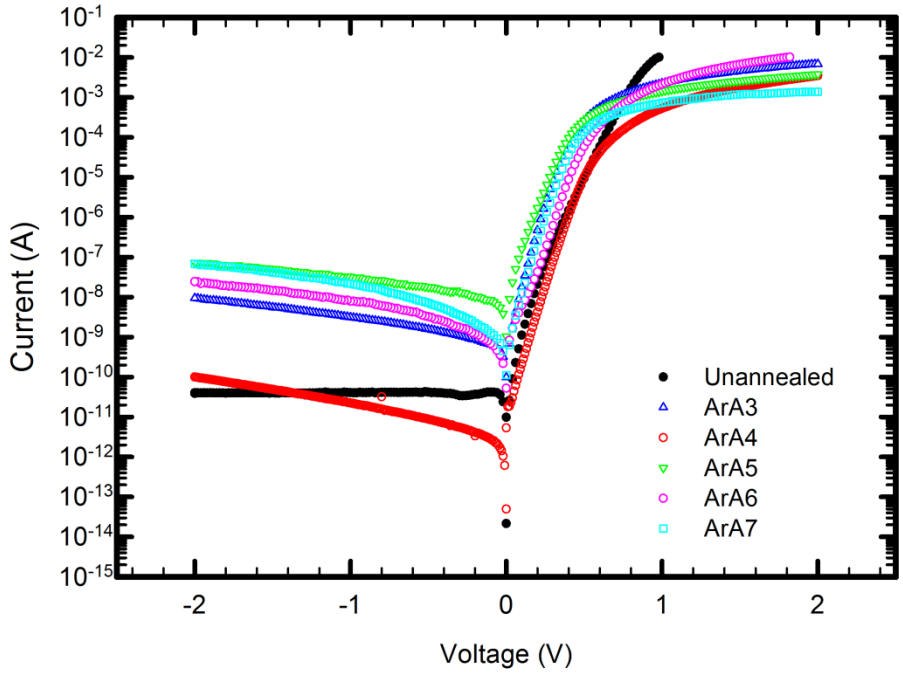

Figure 6.3.3.3.1: Semi-logarithmic IV characteristic of Pd Schottky contacts deposited on argon annealed ZnO. The characteristics were recorded at 298 K in the dark. ArA3, ArA4, ArA5, ArA6 and ArA7 indicate the annealing temperature of 300°C, 400°C, 500°C, 600°C and 700°C, respectively. Figure adopted from ref [8]

Figure 6.3.3.3.1 illustrates the effects of annealing on the IV characteristics of Pd Schottky contacts deposited on ZnO. The annealed samples yield contacts with very high reverse currents compared to the un-annealed contacts. Of particular interest is the reverse current for the 400°C annealed samples. Even though this current increases, it does not differ much from that of the un-annealed samples. These high reverse currents can be explained by considering the defects that are introduced during annealing of the samples. One would expect the 400°C annealed samples to have a low concentration of defects as compared to the 300°C, 500°C 600°C and 700°C annealed samples since defects can also contribute to high leakage currents in metal/semiconductor contacts.

Parameters obtained from the IV characteristics of Figure 6.3.3.3.1 are given in Table 6.3.3.3.1. These have been obtained by fitting the linear part of the forward IV curves to a pure thermionic emission model. The 400°C annealed samples show a very high barrier height compared to all the annealed samples, hence the observed low leakage current. The annealed samples however show an increase in series resistance of the contacts compared to the un-annealed samples. As has been noted with the vacuum annealed and oxygen annealed

samples, the CV barrier height is larger than the IV barrier height and also the net doping concentration for the annealed samples is lower than that of the un-annealed samples.

Table 6.3.3.3.1: *Average values of Schottky barrier height, SBH, ideality factor, series resistance R_s, and the free carrier concentration from CV depth profile, for the un-annealed and oxygen annealed ZnO samples.*

Annealing Temperature(°C)	SBH (eV) *IV*	Ideality factor	R_s (Ω)	SBH (eV) *CV*	N_{dCV} $10^{16}cm^{-3}$
-------	0.74±0.02	1.67 ± 0.01	190	1.16±0.02	26.3±0.3
300	0.70±0.01	1.25 ± 0.07	206±3	1.53±0.06	5.53±0.04
400	0. 81±0.01	1.37 ± 0.07	312±30	1.40±0.06	12.4 ±0.4
500	0.63±0.02	1.72 ± 0.02	391±50	2.55±0.04	6.65±0.01
600	0.74±0.02	1.43± 0.06	110±20	1.45±0.03	10.2±0.03
700	0.73±0.02	1.17± 0.05	(8.4±1)k	0.86±0.02	9.40±0.03

Figure 6.3.3.3.2 shows the DLTS spectra obtained from the un-annealed and argon annealed ZnO samples. The insert shows a new peak observed on the 700°C annealed samples together with the E2 peak. The un-annealed and annealed ZnO samples contain three prominent peaks, E1, E2 and E3. Figure 6.3.3.3.3 also shows DLTS spectra for the un-annealed and argon annealed samples. The insert shows the annealing induced E4 peak on the 300°C, 500°C and 600°C annealed samples. Interesting enough, the 400°C does not show any annealing induced deep level defects.

With all the other annealing temperatures examined in this study, the E4 is observed up to an annealing temperature of 600°C after which it disappears and Ex is induced. The identities of the E4 and Ex deep levels are not known yet. The fact is; E4 and Ex are not thermally induced defects, but they are ambient related defects as they have not been observed in vacuum annealing nor in 300°C, 500°C, 600°C and 700°C oxygen annealing. The Arrhenius plots of Figure 6.3.3.3.4 have been used to calculate the estimated activation enthalpy and capture cross-section for the 700°C annealed samples. The values of the activation enthalpy and apparent capture cross-section for the peaks are given in Table 6.3.3.3.2.

The activation enthalpy of the Ex peak has been estimated to be 167 meV with an apparent capture cross-section of 1×10^{-16} cm^2. A defect with an energy level similar to that of Ex was observed in melt-grown samples by Ye *et al.* [9] after oxygen implantation and subsequent annealing at 750°C in air and Gu *et al* [10] after annealing nitrogen implanted ZnO samples.

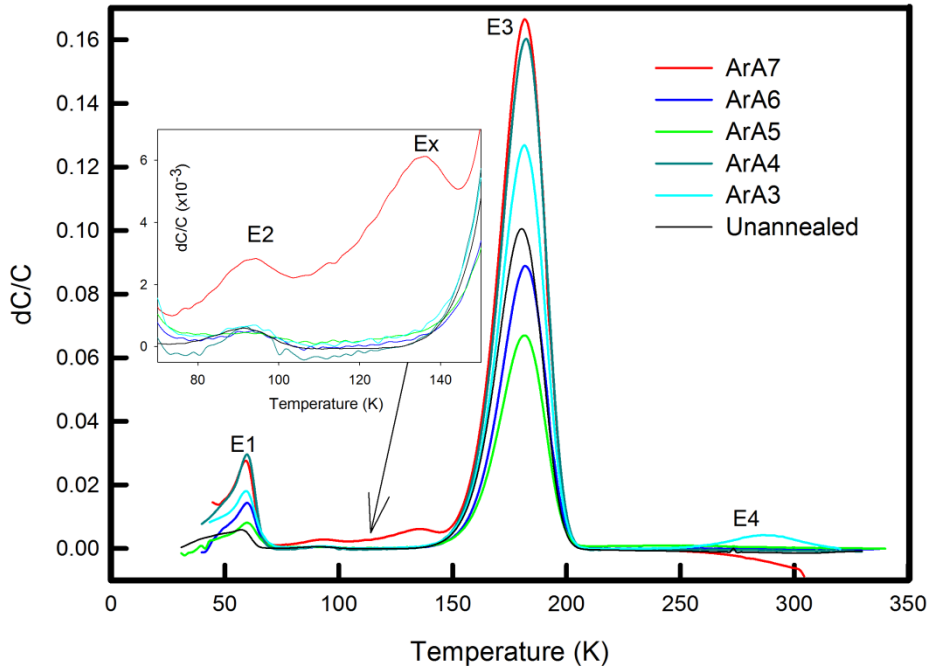

Figure 6.3.3.3.2: DLTS spectra obtained from Pd Schottky contacts deposited on argon annealed ZnO. The spectra were recorded at a quiescent reverse bias of -2.0 V, filling pulse of 0.30 V, filling pulse width of 2 ms and rate window of 100s^{-1} in the temperature range 30 – 350 K. The insert shows the E2 and Ex peaks. ArA3, ArA4, ArA5, ArA6 and ArA7 indicate the annealing temperature of 300°C, 400°C, 500°C, 600°C and 700°C, respectively

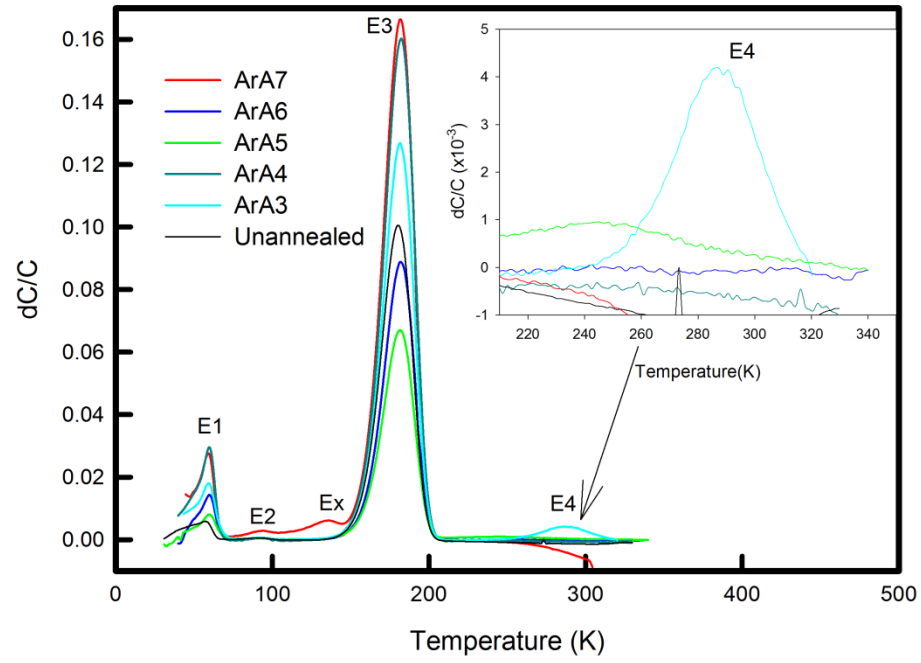

Figure 6.3.3.3.3: DLTS spectra obtained from Pd Schottky contacts deposited on argon annealed ZnO. The spectra were recorded at a quiescent reverse bias of -2.0 V, filling pulse of 0.30 V, filling pulse width of 2 ms and rate window of 100s^{-1} in the temperature range 30 – 350 K. The insert shows the E4 peak. ArA3, ArA4, ArA5, ArA6 and ArA7 indicate the annealing temperature of 300°C, 400°C, 500°C, 600°C and 700°C, respectively

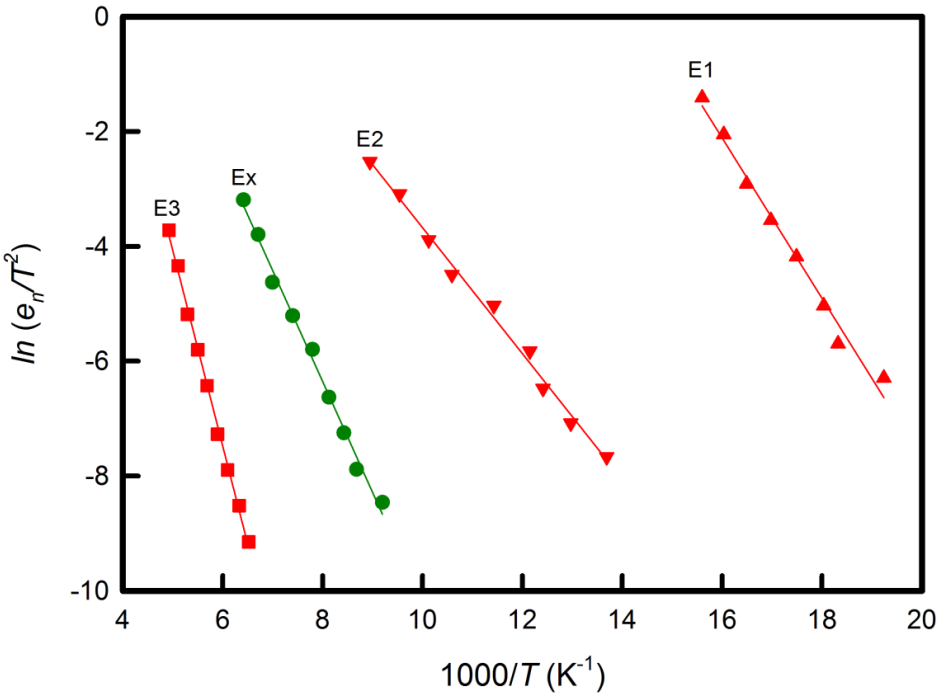

Figure 6.3.3.3.4: Arrhenius plots obtained from Pd Schottky contacts deposited on 700°C argon annealed ZnO.

Table 6.3.3.3.2: *Values of activation enthalpy and capture cross section for the Pd Schottky contacts deposited on un-annealed and 700°C argon annealed ZnO. The activation enthalpy is measured relative to the minimum of the conduction band.*

Annealing temperature (°C)	E1 (meV)	Capture cross section (cm^2)	E2 (meV)	Capture cross section (cm^2)	Ex (meV)	Capture cross section (cm^2)	E3 (meV)	Capture cross section (cm^2)	E4 (meV)	Capture cross section (cm^2)
No anneal	120	5×10^{-12}	100	1×10^{-16}	--------	--------	300	3×10^{-14}	-----	---------
700	120	9×10^{-12}	95	2×10^{-17}	167	1×10^{-16}	293	1×10^{-16}	-----	---------

Of particular interest is the introduction of E4 after annealing ZnO in different ambient conditions. Repeated Ar annealing on several samples from the same batch shows the introduction of E4 at 300°C, 500°C and 600°C and not at 400°C. However, oxygen annealing does not introduce E4 after 300°C, 500°C and 600°C, but it is only observed after annealing ZnO samples at 400°C which is exactly the opposite case for Ar annealing. Figure 6.3.3.3.5 shows the spectra obtained from the 400°C argon annealed and 400°C oxygen annealed samples. The insert shows the E4 peak. The intensity of E3 seems to be affected by the formation of either the Ex or E4 deep level for all the annealing conditions and ambient used in this study. The E4 peak is broad, indicating that it may consist of two or more energy levels which are closely spaced. Laplace-DLTS has been employed to separate these closely

spaced energy levels. Results are presented in the attached publication in section 6.3.4. It must be noted that E4 only refers to the fourth peak that is induced by annealing, not necessarily that the deep level defects introduced during argon annealing at 300°C, 500°C and 600°C and oxygen annealing at 400°C are the same.

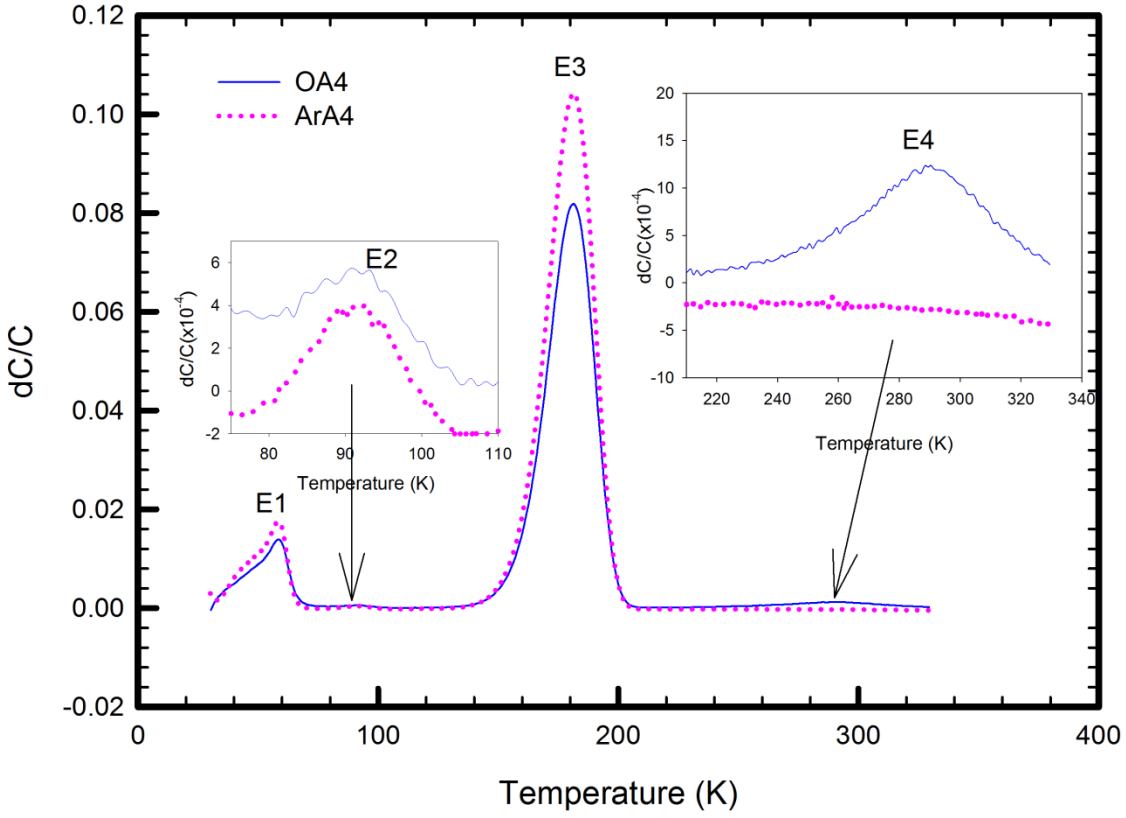

Figure 6.3.3.3.5: DLTS spectrum obtained from Pd Schottky contacts deposited on oxygen and argon annealed ZnO. The spectra were recorded at a quiescent reverse bias of -2.0 V, filling pulse of 0.30 V, filling pulse width of 2 ms and rate window of 100s^{-1} in the temperature range 30 – 350 K. OA4 and ArA4 indicate the sample annealed in oxygen at 400°C and argon at 400°C, respectively. The inserts show the E2 and the E4 peak observed in the oxygen annealed samples.

Since it has been observed that the defects induced through annealing are ambient related and not thermally related, a study of the annealing induced defects at 300°C in different ambient conditions is presented in publication 5 obtained from the link below.

Publication 5: Effects of hydrogen, oxygen, and argon annealing on the electrical properties of ZnO and ZnO devices studied by IV, DLTS and LDLTS

http://dx.doi.org/10.1063/1.4709728

Summary

Based on the findings of this study on annealing induced defects in ZnO, this subject is very complicated since one of the inert gases, i.e. argon can induce defects in ZnO. Identifying the nature of these annealing induced defects is still a subject under investigation. Table 6.3.3.3.3 presents the findings by other authors on the annealing induced defects in ZnO under various ambient conditions.

Table 6.3.3.3.3. *Summary of defects induced in as-received ZnO after annealing in different ambient conditions and temperatures.*

Growth Technique	Annealing Ambient	Annealing temperature (°C)	Defect/s induced	Identity	Ref
Melt	Vacuum	400	--------		This work
		600	--------	---------	This work
		700	--------		This work
	O_2	300	--------	--------	[6]
		400	E4 (0.60 eV)	?	This work
		500	--------	--------	This work
		600	--------	---------	This work
		700	--------	---------	This work
	Ar	300	E4 (0.67 eV)	?	[6]
		400	-------	--------	[8]
		500	E4	?	[8]
		600	E4	?	[8]
		700	Ex (0.16 eV)	?	[8]
	H_2	300	E4 (0.60 eV)	?	[6]
Hydrothermal	O_2 N_2 Ar N_2/H_2	1400 700	E4(0.54 eV)	Zn deficiency related	[11]

Conclusions

Annealing of samples prior to Schottky contact fabrication allows for the determination and characterization of high temperature annealing induced deep level defects in melt grown single crystal ZnO. Within the temperature range studied, i.e. 300°C – 700°C, vacuum annealing does not induce any new defects, neither does it anneal out the prominent defects observed in the as-grown material. Oxygen annealing also does not introduce defects on all the other temperatures, except at 400°C where E4 is induced. The identity of E4 is not known as yet. With Ar annealing, a deep level defect labelled E4 is observed at 300°C, 500°C and 600°C. It must be mentioned that this defect is not the same for the three different annealing temperatures. 400°C Ar annealing does not induce any defect in ZnO and also does not anneal out the E1, E2 and E3 defects. Annealing the ZnO samples in Ar at 700°C results in E4 annealing out and a new deep level defect, Ex being induced. Hydrogen annealing has only been performed at 300°C where a deep level defect labelled E4 has also been induced. Melt grown single crystal ZnO samples annealed in different ambient conditions and temperatures reveal the introduction of defects which are ambient and temperature related. This behaviour of ZnO enables, and is significant for defect engineering within the material where if certain defects with certain properties are required, their introduction can be easily achieved and controlled by either using specific temperature and/or ambient conditions.

References

1. C. R. Crowell and V. L. Rideout, Solid-St. Electron. **12**, 89 (1969)
2. A. K. Srivastava, B. M. Arora, and S. Guha, Solid-St. Electron. **24**, 185 (1981)
3. A. K. Srivastava, and B. M. Arora, Solid-St. Electron. **24**, 1049 (1981)
4. S. M. Sze, Physics of Semiconductor devices, Wiley, New York, 2nd Ed., p.292 (1981)
5. H. von Wenckstern, PhD Thesis, Universitat Leipzig (2008)
6. W. Mtangi, F. D. Auret, W. E. Meyer, M. J. Legodi, P. J. Janse van Rensburg, S. M. M. Coelho, M. Diale, and J. M. Nel, J. Appl. Phys. **111**, 094504 (2012)
7. W. Mtangi, F.D. Auret, P.J. Janse van Rensburg, S. M. M. Coelho, M. J. Legodi, J.M. Nel, W.E. Meyer, J. Appl. Phys. **110**, 094504 (2011)
8. W. Mtangi, F. D. Auret, M. Diale, W. E. Meyer, A. Chawanda, H. de Meyer, P.J. Janse van Rensburg, and J. M. Nel J. Appl. Phys. **111**, 084503 (2012)
9. Z. R. Ye, X. H. Lu, G. W. Ding, C. C. Ling, G. Brauer, and W. Anwand, Semicond. Sci. Technol. **26**, 095016 (2011)
10. Q. L. Gu, C. K. Cheung, C. C. Ling, A. M. C. Ng, A. B. Djurisic, L. W. Lu, X. D. Chen, S. Fung, C. D. Beling and H. C. Ong, J. Appl. Phys. **103**, 093706 (2008)
11. V. Quemener, L. Vines, E. V. Monakhov, and B. G. Svensson, Int. J. Appl. Ceramic. Technol. **8**, 1017 (2011)

6.3.4 Argon and Oxygen annealing

Introduction

Following the results that have been presented in the previous sections, a study has been performed to investigate whether it is possible to anneal out the E4 deep level defect in oxygen ambient at the same temperature at which it has been introduced through argon annealing.

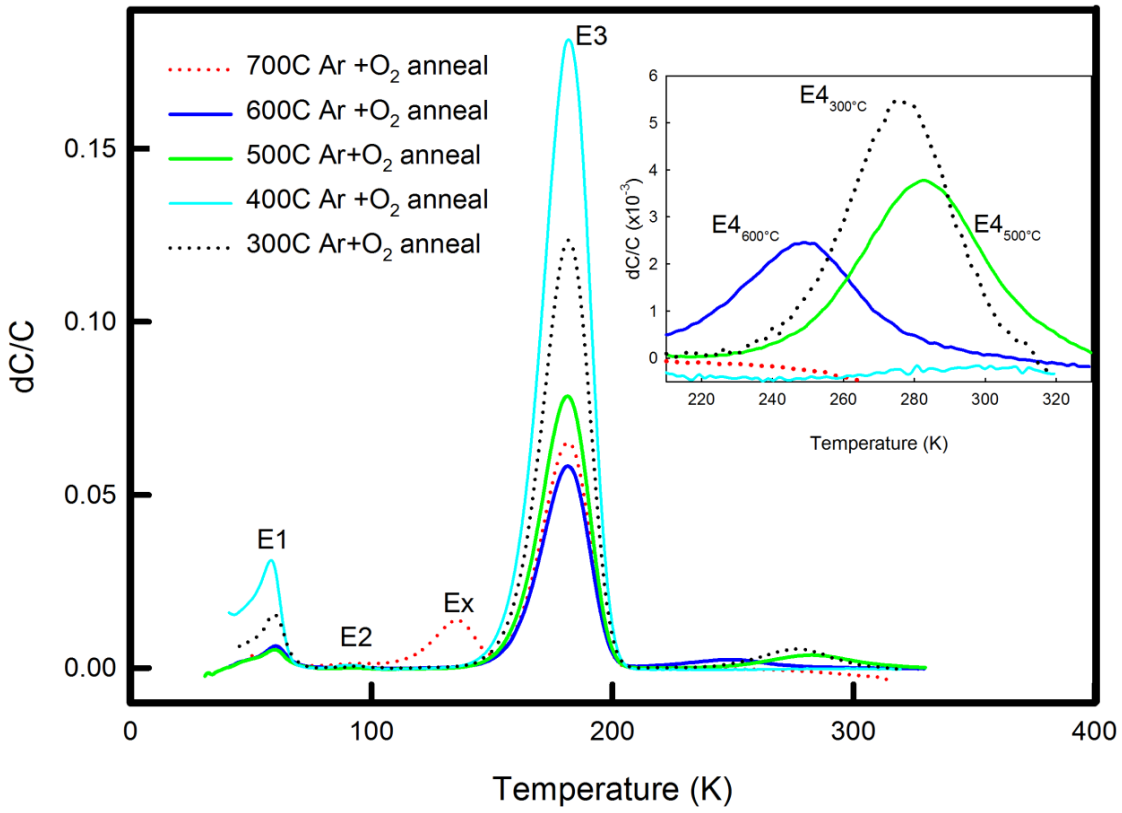

Figure 6.3.4.1: Normalized DLTS spectra of ZnO samples annealed in Ar + O_2 at different temperatures. The spectra were recorded on the 11th of November 2011. The measurement conditions comprised of a quiescent reverse bias of 2.0 V, filling pulse V_p = 0.3 V, filling pulse width of 2.0 ms and a rate window of 100 s^{-1}.

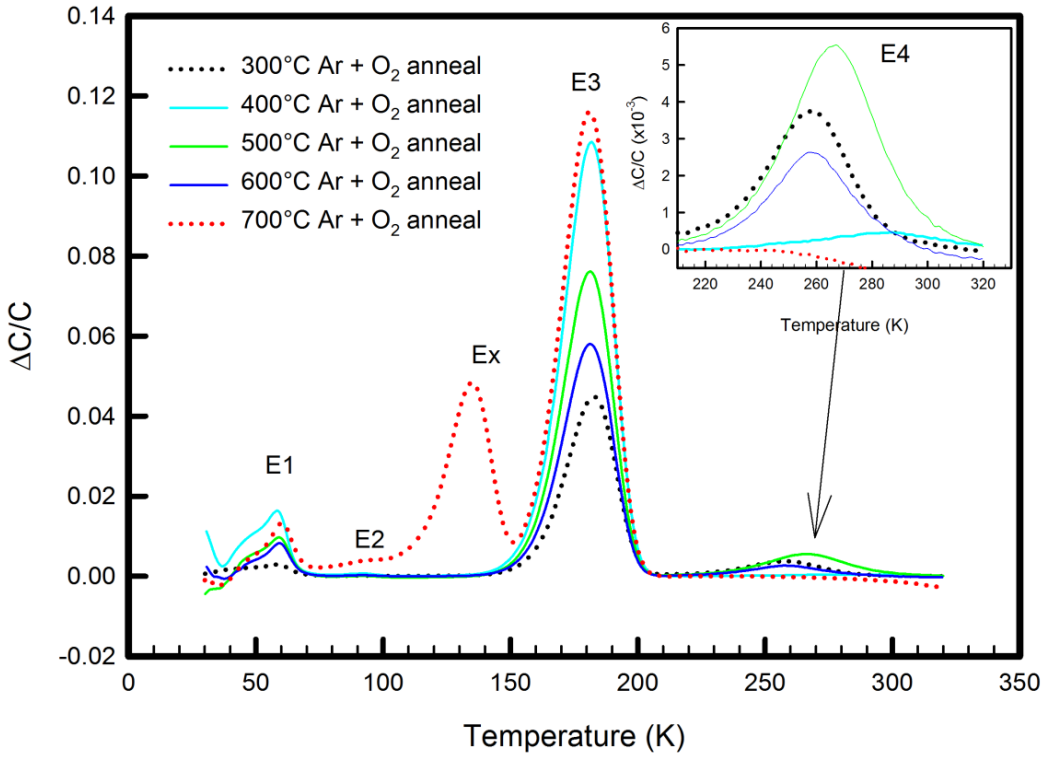

Figure 6.3.4.2: Normalized DLTS spectra of ZnO samples annealed in Ar + O_2 at different temperatures. The spectra were recorded on the 5th of May 2012. The measurement conditions comprised of a quiescent reverse bias of 2.0 V, filling pulse V_p = 0.3 V, filling pulse width of 2.0 ms and a rate window of 100 s^{-1}.

Figure 6.3.4.1 shows the DLTS spectra of the Ar + O_2 annealed samples determined on the 11th of November 2011, while Figure 6.3.4.2 shows the spectra that was obtained on the 5th of May 2012. When the measurements were performed just after contact fabrication, the 400°C Ar + O_2 annealed samples did not show the E4 peak. Six months later, the 400°C annealed sample now shows the E4 peak. All the annealing induced defects indicate a change in either the peak height or the peak position (in terms of temperature). After six months, the intensity of the E4 in the 500°C annealed samples is now higher than that of the 300°C annealed samples. The intensity of the normalized E3 peak for the annealed samples also appears to change with time. It appears as if the E4 peak affects the E3 peak in one way or the other. Using the 400°C annealed sample as an example; when E4 was not present, the intensity of the E3 peak was high (Figure 6.3.4.1). With the E4 peak appearing, the intensity of E3 decreases (Figure 6.3.4.2). For the 400°C Ar annealed samples fabricated on the same day (Figure not shown), after the same number of months, E4 is still not present. Hence O_2 is responsible for the E4 peak that has been observed in the 400°C Ar + O_2 annealed samples.

Figure 6.3.4.3 shows the Arrhenius plots for the annealing induced defects in the Ar + O2 annealed samples. The values of the estimated activation enthalpies and apparent capture cross-sections are presented in Table 6.3.4.1.

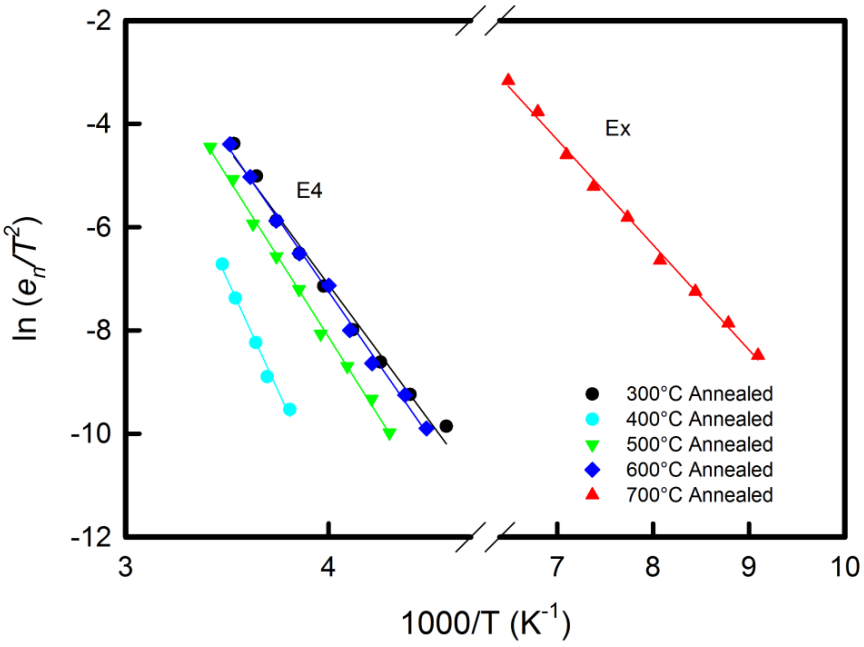

Figure 6.3.4.3: Arrhenius plots for the annealing induced defects in ZnO after Ar + O_2 annealing.

Table 6.3.4.1*: Values of annealing temperature, estimated activation enthalpy and apparent capture cross-section for the annealing induced defects in ZnO from measurements performed on 5 May 2012.*

Annealing Temperature (°C)	Activation enthalpy (meV)	Apparent capture cross-section (cm^2)
300	E4(460)	2×10^{-14}
400	E4(740)	2×10^{-10}
500	E4(540)	3×10^{-13}
600	E4(490)	7×10^{-14}
700	Ex(160 – 180)	3×10^{-16}

From the Arrhenius plots, the estimated activation enthalpy and apparent capture cross-section, it can be clearly observed that the defect labelled E4 is not the same for the 300°C, 400°C and 600°C.

More details on the Ar + O_2 studies are presented in publication 6 obtained from the provided link. The publication outlines the experimental procedure, results and discussions and conclusions drawn from this investigation.

Publication 6: Effects of high temperature annealing on single crystal ZnO and ZnO devices

http://dx.doi.org/10.1063/1.3700186

Summary

Annealing melt grown single crystal ZnO in Ar ambient at high temperatures introduces deep level defects. These deep levels tend to affect the electrical properties of the Schottky contacts fabricated on the annealed material by increasing the reverse leakage current and the series resistance of the contacts. DLTS measurements performed on ZnO material annealed at different temperatures reveal different deep level defects induced at those particular temperatures. An increase in annealing temperature results in a transformation of the observed deep level defects. Below the annealing temperature of 700°C, a deep level defect labelled E4 appeared in the DLTS spectra slightly below room temperature. After 700°C annealing, the E4 deep level defect anneals out and a new low temperature deep level defect, Ex is induced. These deep levels can be said to be unstable as they show some changes in the temperature peak position with time. These changes could be due to changes in the environmental conditions, particularly the temperature at which the samples are kept, which in this particular study is room temperature. For the 400°C Ar + O_2 annealed samples, the E4 deep level defect, which is not observed just after contact fabrication, is observed after a period of time, in this case, six months. This might be a result of room temperature annealing of the samples which activates some defect species. However the E4 deep level is not induced in the 400°C Ar annealed samples kept in the same environment for the same amount of time. The question is: (i). what does Ar annealing do to the samples? (ii). what is the effect of oxygen annealing on Ar annealed ZnO samples? This question is yet to be answered after further investigations.

6.4 Irradiation induced defects

Introduction

ZnO has the potential to be used in the fabrication of UV detectors and space applications. In space applications, devices often operate in harsh radiation conditions which comprise of highly energetic particles and elevated temperatures. This requires the material to be highly resistant to radiation damage for devices to operate reliably for extended periods. In this section, the effects of exposing Pd Schottky contacts to H^+ ion irradiation are presented.

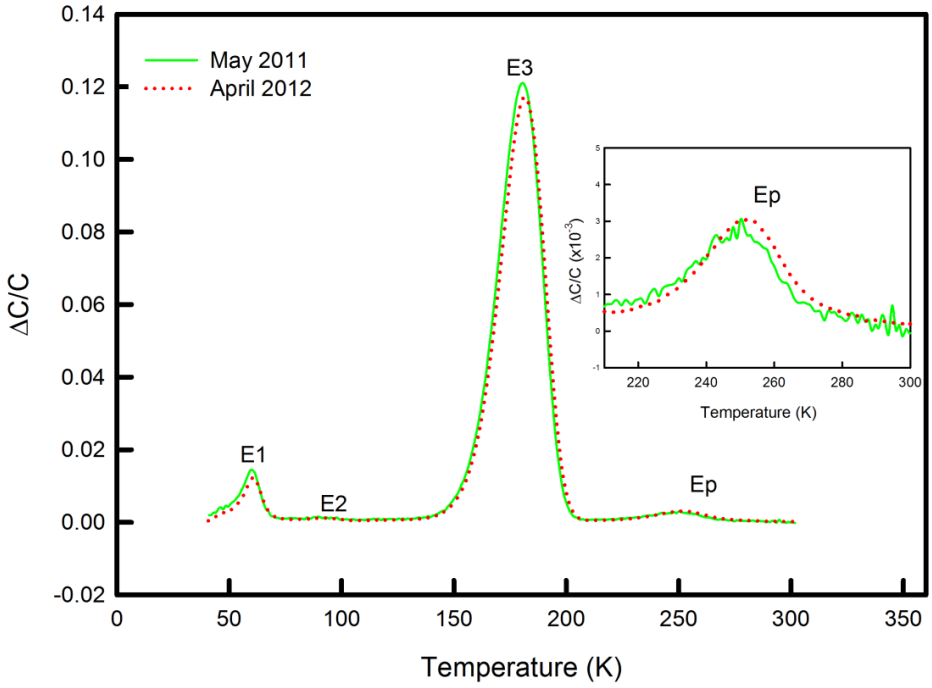

Figure 6.4.1: *DLTS spectra for the proton irradiated Pd/ZnO Schottky contacts. These spectra were recorded at a quiescent reverse bias of 2.0 V, V_p = 0.3 V and filling pulse width of 2.0 ms and rate window of 100 s^{-1}. The green solid line shows the spectrum recorded in May 2011, while the red dotted line indicates the spectrum obtained in April 2012.*

Figure 6.4.1 shows the DLTS spectra of the 1.6 MeV proton irradiated ZnO samples. The spectra show three prominent peaks that have also been observed in the as-grown samples. An extra peak labelled Ep has been introduced by proton irradiation. The estimated activation enthalpy and capture cross-sections are given in the Arrhenius plots of Figure 6.4.2. The proton induced defect has an activation enthalpy of 533 meV and an apparent capture cross-section of about $1 \times 10^{-12}\text{cm}^2$. A defect with almost the same energy level was observed by

Auret *et al.*[1] in SCVT grown samples after 1.8 MeV proton irradiation. In their study, they report an activation enthalpy of Ep1 to be 0.54 ± 0.02 eV and an apparent capture cross-section of $(3.0 \pm 1.0) \times 10^{-13}\text{cm}^2$. Schmidt [2] also reported a defect which he labelled E4 in ZnO thin films after 1.6 MeV proton irradiation, with activation energy of 0.55 eV. There is therefore a high possibility that the Ep defect is the same as the Ep1 observed by Auret *et al.* [1] and the E4 observed by Schmidt [2]. As shown in Figure 6.4.1, the Ep defect shows high stability for a sample kept at room temperature conditions. The spectra recorded after almost a year indicates the presence of Ep with almost the same concentration.

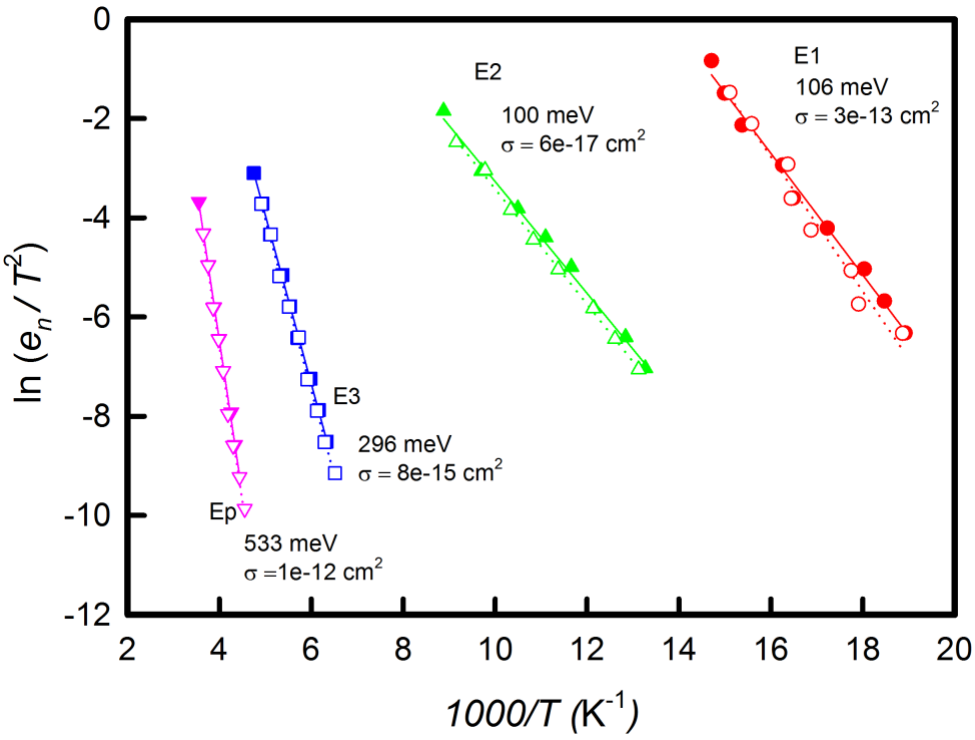

Figure 6.4.2: Arrhenius plots obtained from the 1.6 MeV proton irradiated Pd/ZnO Schottky contacts. Filled symbols indicate the measurements performed in May 2011 while the empty symbols represent the data obtained in April 2012.

The stability of the Ep defect is also illustrated using the depth profile of Figure 6.4.3. This profile was recorded at a constant reverse bias of 2.0 V and increasing pulses in steps of 0.1 V. As demonstrated in Figure 6.4.3, the concentration at any given depth for the sample evaluated in May 2011 is slightly higher than the concentration determined in April 2012, but to within experimental error these values are almost the same. This clearly indicates that once introduced, the Ep1 is stable for the period specified in this study. The same is observed for the E1, E2 and E3 peaks as illustrated in the Arrhenius plots of Figure 6.4.2.

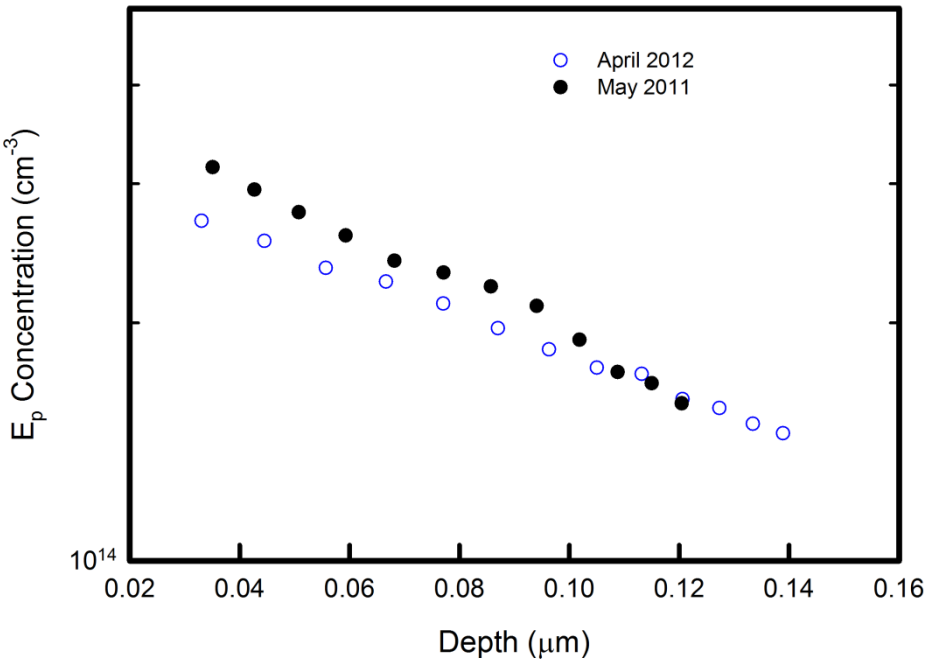

Figure 6.4.3: Variation of trap concentration with depth obtained from the irradiation induced E_p peak observed in Pd/ZnO Schottky contacts.

Summary

Exposing ZnO to highly energetic particles introduces a new deep level defect. However this defect exists in low concentration indicating that ZnO is resistant to radiation damage to some extent. The irradiation induced peak has proved to be stable within the period evaluated within this particular study. Introduction of Ep after irradiation has no effect on the other peaks already present in the material.

References

1. F.D. Auret, S.A. Goodman, M. Hayes, M.J. Legodi, H.A. van Laarhoven, and D.C. Look, Appl. Phys. Lett., **79**, 3074 (2001)
2. M. Schmidt, PhD Thesis, Leipzig University (2011)